OPEN ACCESS Freely available online

PLOS ONE

Knockout of Endothelial Cell-Derived Endothelin-1 Attenuates Skin Fibrosis but Accelerates Cutaneous Wound Healing

Katsunari Makino[1]*, Masatoshi Jinnin[1], Jun Aoi[1], Ikko Kajihara[1], Takamitsu Makino[1], Satoshi Fukushima[1], Keisuke Sakai[1], Kazuhiko Nakayama[2], Noriaki Emoto[2], Masashi Yanagisawa[3,4], Hironobu Ihn[1]

1 Department of Dermatology and Plastic Surgery, Faculty of Life Sciences, Kumamoto University, Kumamoto, Japan, **2** Clinical Pharmacy, Kobe Pharmaceutical University, Kobe, Japan, **3** Department of Molecular Genetics and Howard Hughes Medical Institute, University of Texas Southwestern Medical Center, Dallas, Texas, United States of America, **4** International Institute for Integrative Sleep Medicine (WPI-IIIS) and Center for Behavioral Molecular Genetics, University of Tsukuba, Tsukuba, Japan

Abstract

Endothelin (ET)-1 is known for the most potent vasoconstrictive peptide that is released mainly from endothelial cells. Several studies have reported ET-1 signaling is involved in the process of wound healing or fibrosis as well as vasodilation. However, little is known about the role of ET-1 in these processes. To clarify its mechanism, we compared skin fibrogenesis and wound repair between vascular endothelial cell-specific ET-1 knockout mice and their wild-type littermates. Bleomycin-injected fibrotic skin of the knockout mice showed significantly decreased skin thickness and collagen content compared to that of wild-type mice, indicating that bleomycin-induced skin fibrosis is attenuated in the knockout mice. The mRNA levels of transforming growth factor (TGF)-β were decreased in the bleomycin-treated skin of ET-1 knockout mice. On the other hand, skin wound healing was accelerated in ET-1 knockout mice, which was indicated by earlier granulation tissue reduction and re-epithelialization in these mice. The mRNA levels of TGF-β, tumor necrosis factor (TNF)-α and connective tissue growth factor (CTGF) were reduced in the wound of ET-1 knockout mice. In endothelial ET-1 knockout mouse, the expression of TNF-α, CTGF and TGF-β was down-regulated. Bosentan, an antagonist of dual ET receptors, is known to attenuate skin fibrosis and accelerate wound healing in systemic sclerosis, and such contradictory effect may be mediated by above molecules. The endothelial cell-derived ET-1 is the potent therapeutic target in fibrosis or wound healing, and investigations of the overall regulatory mechanisms of these pathological conditions by ET-1 may lead to a new therapeutic approach.

Citation: Makino K, Jinnin M, Aoi J, Kajihara I, Makino T, et al. (2014) Knockout of Endothelial Cell-Derived Endothelin-1 Attenuates Skin Fibrosis but Accelerates Cutaneous Wound Healing. PLoS ONE 9(5): e97972. doi:10.1371/journal.pone.0097972

Editor: Bernhard Ryffel, French National Centre for Scientific Research, France

Received February 11, 2014; **Accepted** April 25, 2014; **Published** May 22, 2014

Funding: This study was supported in part by a grant for scientific research from the Japanese Ministry of Education, Science, Sports and Culture, and by project research on intractable diseases from the Japanese Ministry of Health, Labour and Welfare. The funders had no role in study design, data collection and analysis, decision to publish, or preparation of the manuscript.

Competing Interests: The authors have declared that no competing interests exist.

* E-mail: mjin@kumamoto-u.ac.jp

Introduction

Endothelin-1 (ET)-1, one of the three members of ET family, is known as the most potent vasoconstrictive peptide. The molecule is released mostly from endothelial cells [1,2], and its biological actions are mediated by two different receptors, ET_A and ET_B [3]. In addition to its effect as a vasoconstrictor, ET-1 can stimulate smooth muscle cell proliferation [4]. Furthermore, the molecule induces the expression of several proto-oncogenes such as c-myc or c-fos [5]. Through such diverse biological activities, ET-1 signal is thought to play central roles in several pathological conditions including pulmonary hypertension.

ET-1 is also found to induce collagen expression in cultured fibroblasts of heart, skin or kidney [6–8]. In addition, bosentan, an antagonist of dual ET receptors, reduced the number of digital ulcers in patient with systemic sclerosis, an autoimuune disorder characterized by tissue fibrosis of the skin and internal organs [9]. These results indicate ET-1 signal also has a profibrotic effect *in vitro* and *in vivo*. On the other hand, several researches suggested the drug improves skin fibrosis of systemic sclerosis [10]. Thus, detailed mechanism of ET-1 effects on fibrosis and wound heal is still to be clarified.

Homozygous deletion of ET-1 in mice shows early postnatal lethality caused by craniofacial abnormalities [11]. Therefore, considering that the major source of ET-1 is endothelial cells, we utilized endothelial cell-specific ET-1 knockdown mice for analyzing the mechanism of ET-1 involvement in the skin fibrosis and wound healing.

Materials and Methods

Ethics Statement

All animal experimental protocols in this study were approved by the Committee on the Animal Research at Kumamoto University (Permit Number: 24–150). All efforts were made to minimize suffering.

Mice

Eight-week-old heterozygous ET-$1^{f/f}$; Tie-2-Cre (+) mice and control ET-$1^{f/f}$; Tie-2-Cre (−) littermates (WT, wild-type mice) were used for experiments. ET-$1^{f/f}$; Tie-2-Cre (+) mice were generated as described [12,13]. In brief, mice strains with ET-1 exon 2 flanked by loxP sites were prepared. Tie2-Cre transgenic mice expressing Cre recombinase in a pan-endothelial fashion were utilized for vascular endothelium-specific targeting. By breeding those mice, genetically modified mice depleting the preproET-1 gene specifically in endothelial cells were obtained. The mice were housed in a specific pathogen-free and temperature-controlled environment with a 12-hour light/dark cycle and were fed a standard diet and water *ad libitum*. They did not display any evidence of infection throughout the study. In all experiment, the sex ratio was same between groups.

Bleomycin-induced skin fibrosis in mice

Bleomycin treatment was performed as previously reported [14]. In brief, bleomycin (Nippon Kayaku) was dissolved in phosphate buffered saline (PBS) at a concentration of 1 mg/ml and sterilized by filtration. Bleomycin (100 μl) was injected intradermally into the shaved back of the 8-week-old mice daily for 4 weeks. The back skin was removed on day after final bleomycin injection.

Wound healing experiment

Under the local anesthesia, one full-thickness excisional wound was generated on the dorsal skin using an 8 mm diameter dermal punch. After wounded, mice were caged individually. The wound and surrounding tissue were collected at days 0, 3, 7, 12 post-wounding.

Staining

Skin samples were paraffin-embedded, and sections were dewaxed in xylene and rehydrated in graded alcohols. Haematoxylin and eosin (HE) staining or Masson's trichrome staining was performed as described previously [15].

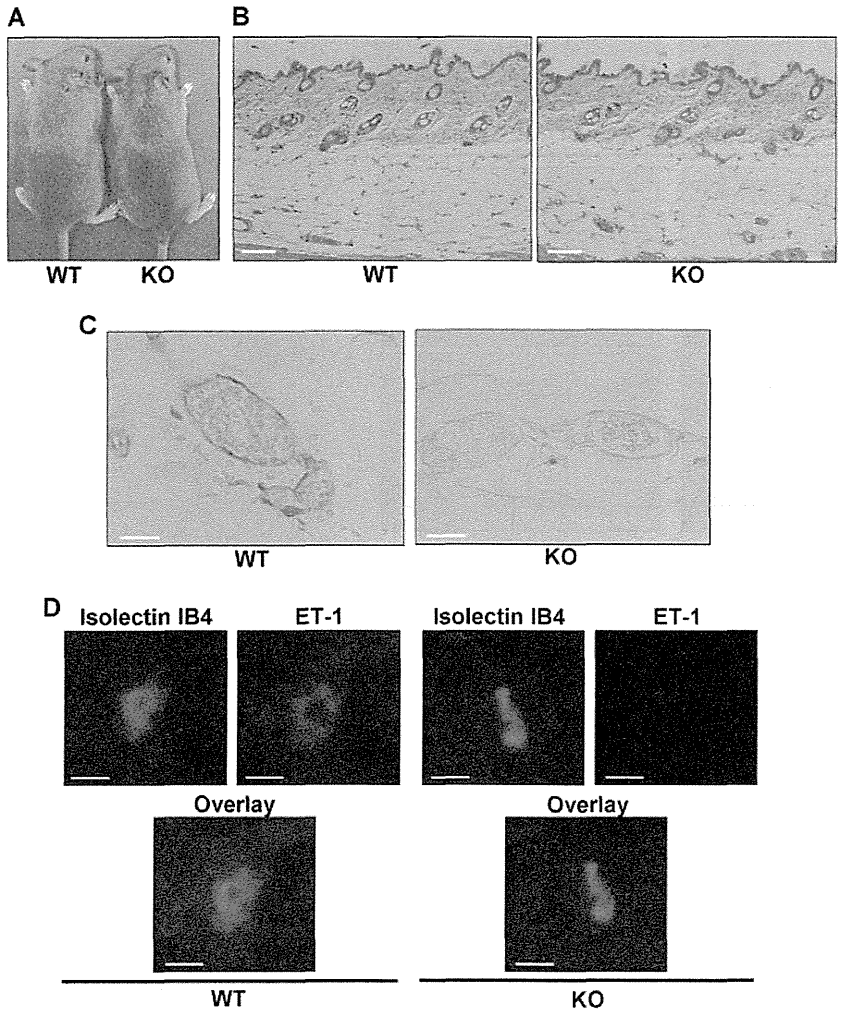

Figure 1. Comparison of the ET-1 expression between wild-type and ET-$1^{f/f}$; Tie-2-Cre (+) mice skins. (A) Gross comparison of a wild-type (WT) and an ET-$1^{f/f}$; Tie-2-Cre (+) (KO) mouse at 8 weeks. (B) Representative haematoxylin and eosin (HE) staining of skin section from a wild-type (WT) and an ET-$1^{f/f}$; Tie-2-Cre (+) (KO) mouse. (C) Representative ET-1 staining of subcutaneous blood vessels in a wild-type (WT) and an ET-$1^{f/f}$; Tie-2-Cre (+) (KO) mouse. Scale bar = 20 μm. (D) Dermal vessels of wild-type (WT) and ET-$1^{f/f}$; Tie-2-Cre (+) (KO) mice were stained with antibodies against isolectin IB4 (green) and ET-1 (red). Scale bar = 10 μm.
doi:10.1371/journal.pone.0097972.g001

For immunostaining, antigens were retrieved by incubation with proteinase K (DAKO) for 6 minutes. Endogenous peroxidase activity was inhibited, after which sections were blocked with 3% bovine serum albumin (BSA, Sigma) for 20 minutes and then reacted with the primary antibodies for ET-1 (1:250, Peninsula Laboratories), myeloperoxidase (1:100, Thermo), F4/80 (1:100, Abcam), or CD3 (1:100, Serotec) overnight at 4°C. After excess antibody was washed out with PBS, sections were incubated with appropriate HRP-labeled secondary antibody (Nichirei) for 60 minutes at 20°C. The reaction was visualized by diaminobenzidine substrate system (Dojin). Slides were counterstained with Mayer's haematoxylin, and examined under a light microscope (OLYMPUS).

Immunofluorescence

Paraffin sections were deparaffinized in xylen and rehydrated in a graded ethanol series. Antigens were retrieved by incubation with proteinase K for 5 minutes. The slides were blocked in 3% BSA for 60 minutes. As the primary antibodies, rabbit anti-ET-1 polyclonal antibody (1:250, Peninsula Laboratories) and Isolectin IB4 Alexa Fluor 488 dye conjugate (1:200, Invitrogen) were applied to the sections overnight at 4°C [16,17]. After excess antibody was washed out with PBS, a species-matched Alexa 546-labeled secondary antibody (Invitrogen) was added. After 1 hour at room temperature, sections were washed and mounted with VECTASHIELD mounting medium (Vector). Fluorescence images of Alexa 488 and Alexa 546 were recorded with Biozero BZ-8000 fluorescence microscope (KEYENCE).

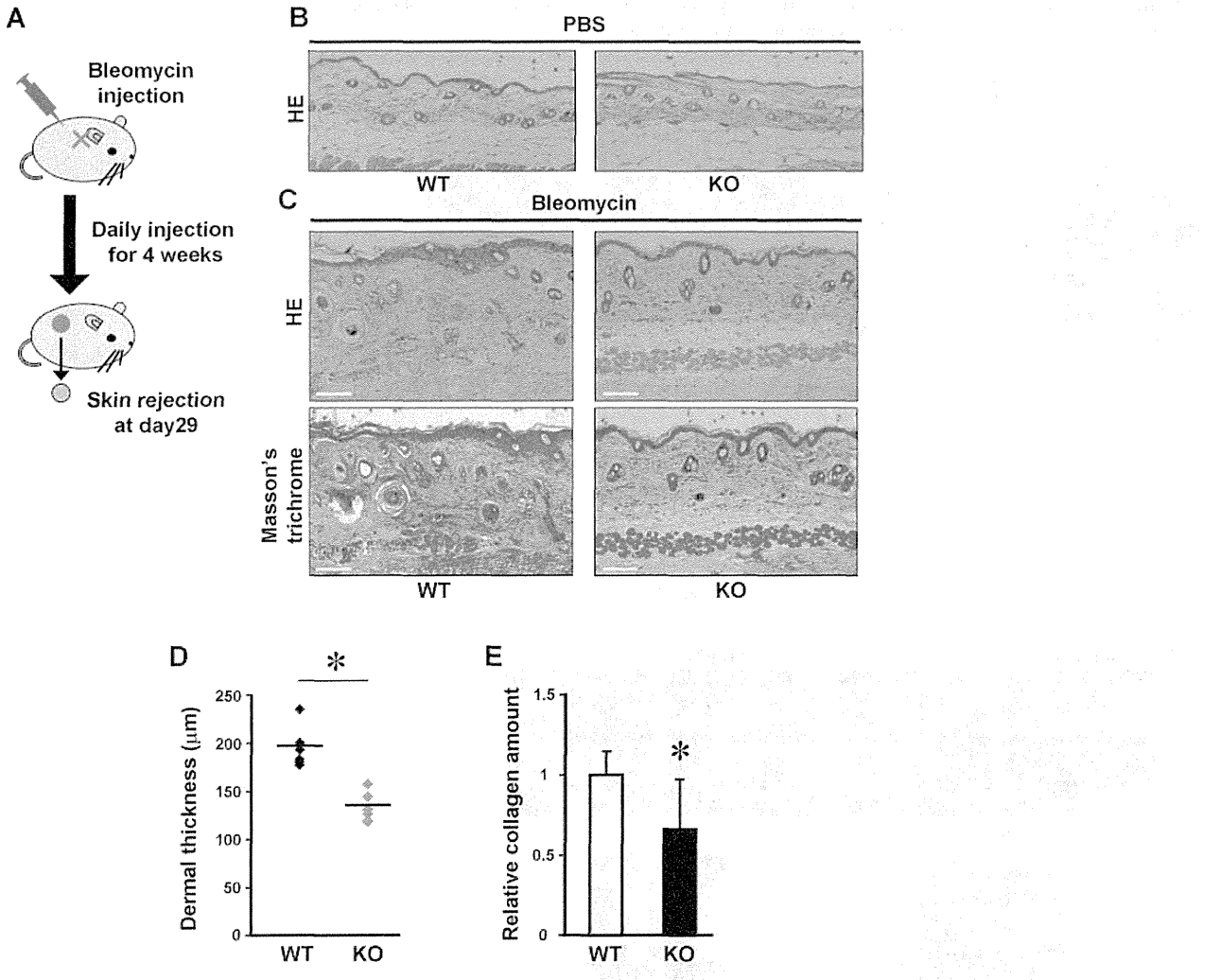

Figure 2. Bleomycin-induced skin fibrosis in wild-type and ET-1$^{f/f}$; Tie-2-Cre (+) mice. (A) The protocol for Figure 2B and 2C is shown. Bleomycin or PBS was locally injected in the back of the wild-type (WT) and ET-1$^{f/f}$; Tie-2-Cre (+) (KO) mice daily for 4 weeks. The back skin was obtained on day 29. (B) Hematoxylin and eosin (HE) staining of PBS-treated mice skin. WT; wild-type, KO; ET-1$^{f/f}$; Tie-2-Cre (+). Scale bar = 100 μm. (C) HE (upper panels) and Masson's trichrome staining (lower panels) of bleomycin-treated mice skin. WT; wild-type, KO; ET-1$^{f/f}$; Tie-2-Cre (+). Scale bar = 100 μm. (D) Dermal thickness of the wild-type (WT) and ET-1$^{f/f}$; Tie-2-Cre (+) (KO) mice was evaluated by measuring the distance between the epidermal-dermal junction and the dermal-fat junction in HE sections under 100-folds magnification. Data are shown on the ordinate (n = 6). Bars show means. *P<0.05. (E) Relative collagen contents of paraffin-embedded sections from the wild-type (WT) and ET-1$^{f/f}$; Tie-2-Cre (+) (KO) mice were determined as described in "Materials and Methods" (n = 6). *P<0.05.
doi:10.1371/journal.pone.0097972.g002

Measurement of collagen contents in tissue sections

Collagen contents in paraffin-embedded skin sections were determined using quantitative micro-assay kit (Chondrex) following the manufacturer's instructions. This method is based on the selective binding of Sirius Red and Fast Green to collagens and non-collagen proteins, respectively [18]. Briefly, 10 μm-thick sections were deparaffinized, and stained with Sirius Red and Fast Green. The color in the tissue sections was eluted by dye extraction solution. Absorbance was measured in a spectrophotometer at OD540 (for Sirius Red) and OD605 (for Fast Green), respectively. The amounts of collagen and non-collagenous proteins in each section were determined by interpolation from a standard curve.

RNA isolation and real-time PCR

Total RNAs were extracted from skin samples using ISOGEN (Nippon Gene). First-strand cDNA was synthesized by PrimeScript RT reagent Kit (Takara). Quantitative real-time PCR was performed on Takara Thermal Cycler Dice (TP800®) using primers and templates mixed with the SYBR Premix Ex Taq II Kit (Takara). Primer sets for transforming growth factor (TGF)-β1, TGF-β3, α2 (I) collagen, connective tissue growth factor (CTGF), Tumor necrosis factor (TNF)-α, E-selectin and glyceraldehyde 3-phosphate dehydrogenase (GAPDH) were purchased from Takara. DNA was amplified for 40 cycles of denaturation for 5 seconds at 95°C and annealing for 30 seconds at 60°C. Data generated from each PCR reaction were analyzed using Thermal Cycler Dice Real Time System ver 2.10B (Takara). The relative fold change of each gene was calculated by standard curve method. Transcript level of gene of interest was normalized to that of GAPDH in the same sample.

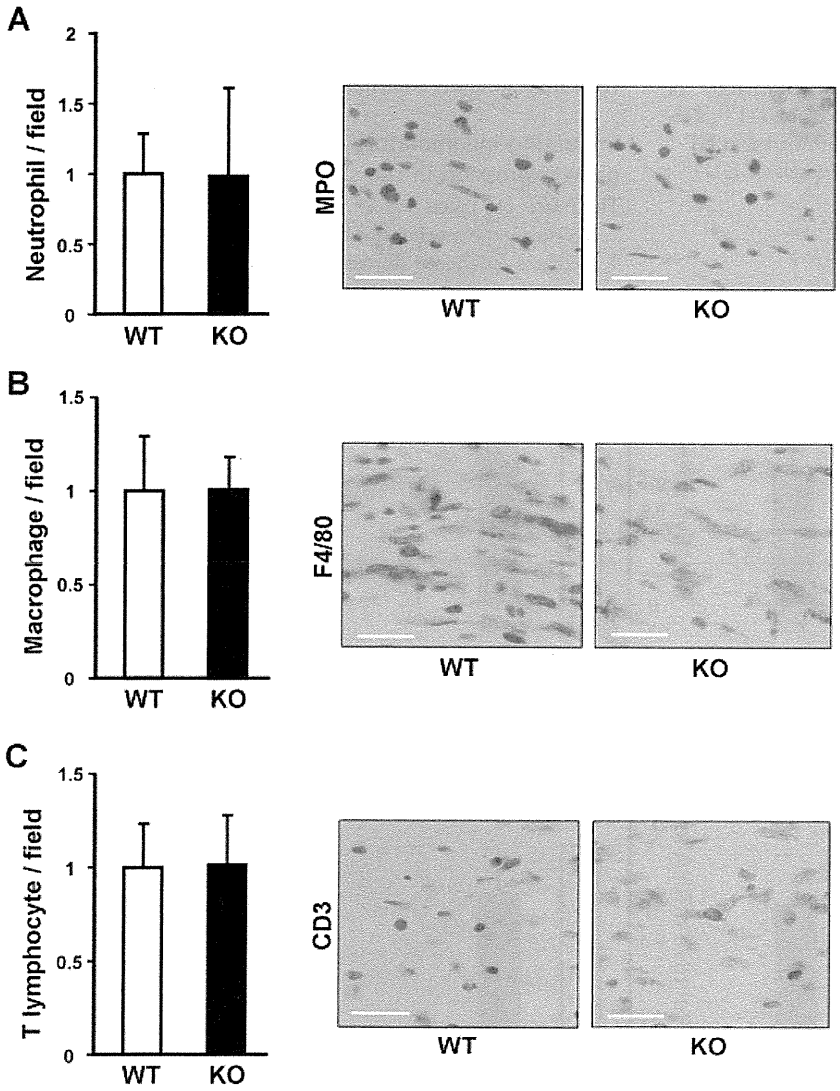

Figure 3. Infiltrating cells in the bleomycin-treated skin of the wild-type (WT) and ET-1$^{f/f}$; Tie-2-Cre (+) (KO) mice. Myeloperoxidase (A), F4/80 (B) and CD3 (C) were stained. Positive cells were counted in five random high-power fields (0.06 mm^2, magnification, ×400). Data were expressed as the mean ± SD of six independent counts (left panel). The representative results of immunostaining for myeloperoxidase, F4/80 and CD3 are shown (right panel).
doi:10.1371/journal.pone.0097972.g003

Statistical analysis

The statistical analysis was carried out with Mann-Whitney U test for the comparison of medians. All analyses were performed with Statcel3 software (OMS). P values <0.05 were considered to be significant.

Results

Expression of ET-1 in the skin of ET-1$^{f/f}$; Tie-2-Cre (+) mice

ET-1 whole-body knockout mice were dead shortly after birth, while the heterozygote ET-1$^{f/f}$; Tie2-Cre (+) mice were born with no defects and grew up without apparent abnormalities [11,12]. As an initial experiment, we compared a skin phenotype of ET-1$^{f/f}$; Tie-2-Cre (+) mice and WT mice. The macroscopic appearance was similar between these mice (Fig. 1A). Additionally, the microscopic skin appearances of ET-1$^{f/f}$; Tie-2-Cre (+) mice were not different from those of WT mice (Fig. 1B).

We then confirmed the expression of ET-1 peptide in vascular endothelial cells of the dorsal skin. By immunohistochemical staining, ET-1 was observed in vessels of WT mice, but not in ET-1$^{f/f}$; Tie-2-Cre (+) mice (Fig. 1C). Similarly, immunofluorescence revealed co-staining of ET-1 and Isolectin IB4, a marker of endothelial cells, in WT mice (Fig. 1D left), but not in ET-1$^{f/f}$; Tie-2-Cre (+) mice (Fig. 1D right). Therefore, we confirmed that ET-1 was successfully knocked-out in the skin blood vessels of ET-1$^{f/f}$; Tie-2-Cre (+) mice.

Bleomycin-induced skin fibrosis in ET-1$^{f/f}$; Tie-2-Cre (+)

Based on above results, we first determined the possibility that the knockout of endothelial cell-derived ET-1 affects the onset of skin fibrosis. As shown in Fig. 2A, skin fibrosis was induced on the back of mice skin by intradermal bleomycin injection daily for 4 weeks. Then, the back skin was removed one day after the final bleomycin injection.

When PBS was injected in back skin as the control, the skin structure and dermal thickness did not differ between ET-1$^{f/f}$; Tie-2-Cre (+) and WT mice (Fig. 2B). In WT mice, the skin injected with bleomycin showed dermal fibrosis with thickened dermis, increased number of collagen bundles and strong Masson's trichrome staining (Fig. 2C left). On the other hand, the bleomycin-treated skin of ET-1$^{f/f}$; Tie-2-Cre (+) mice showed the thinner dermal thickness and weaker Masson's trichrome staining in the dermis, (Fig. 2C right), as compared to those of WT mice. We confirmed such improvement of bleomycin-induced dermal thickening in ET-1$^{f/f}$; Tie-2-Cre (+) mice was statistically significant (Fig. 2D). Consistently, the collagen contents in bleomycin-treated skin of ET-1$^{f/f}$; Tie-2-Cre (+) mice was significantly lower than those in WT mice (Fig. 2E). Therefore, ET-1 may positively contribute to the development of skin fibrosis.

Infiltrating inflammatory cell profile and ECM-related gene expression in the skin of bleomycin-treated ET-1$^{f/f}$; Tie-2-Cre (+) mice

To clarify the mechanism by which endothelial cell-derived ET-1 mediates cutaneous fibrosis, we then compared the number of

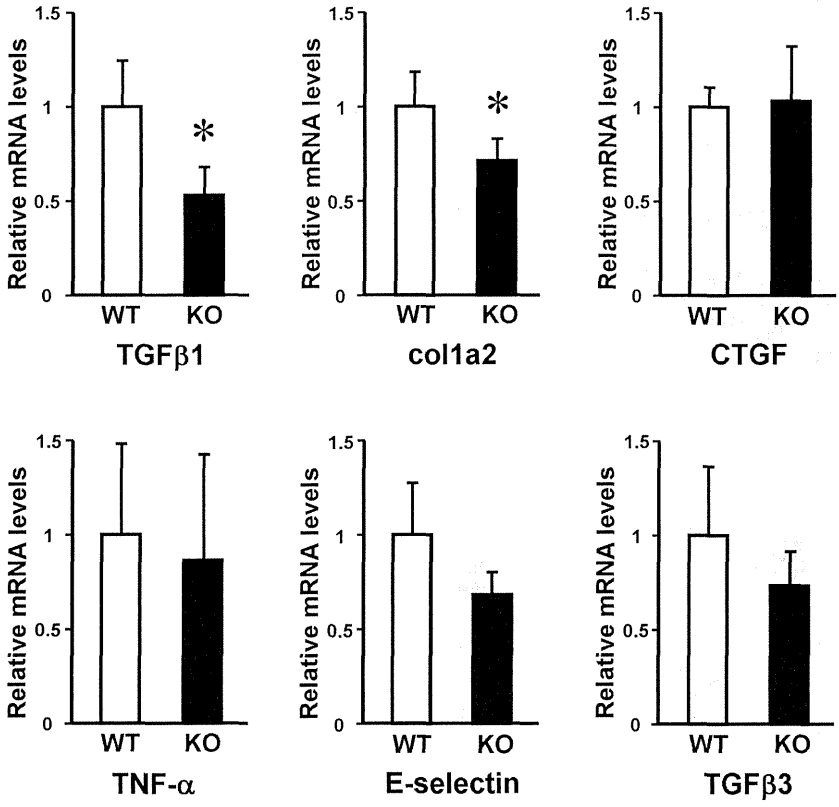

Figure 4. Cytokine expression in the bleomycin-treated skin from the wild-type (WT) and ET-1$^{f/f}$; Tie-2-Cre (+) (KO) mice. Total RNA was extracted from the skin, and the mRNA expression levels of indicated cytokines were determined by real-time PCR. Data are expressed as the mean ± SD of six independent experiments. *P<0.05 as compared with the value in WT mice (1.0).
doi:10.1371/journal.pone.0097972.g004

inflammatory cells in bleomycin-induced fibrotic skin between ET-$1^{f/f}$; Tie-2-Cre (+) mice and WT mice. Myeloperoxidase-positive neutrophils, F4/80-positive macrophages, or CD3-positive T cells were counted in immunohistochemical staining sections. No differences between these mice were seen in the number of neutrophils (Fig. 3A), macrophages (Fig. 3B) and T cells (Fig. 3C).

In addition, we compared the expression of various ECM-related molecules in the bleomycin-treated skin of WT mice and ET-$1^{f/f}$; Tie-2-Cre (+) mice by quantitative real-time PCR (Fig. 4). ET-$1^{f/f}$; Tie-2-Cre (+) mice skin showed significantly decreased mRNA levels of TGF-β1 and α2 (I) collagen relative to WT mice. In contrast, the mRNA levels of TGF-β3, CTGF, TNF-α and E-selectin were not different between these mice. Before the treatment, these levels in the dorsal skin were similar between ET-$1^{f/f}$; Tie-2-Cre (+) and WT mice (data not shown). Thus, our results indicated that decreased mRNA levels of TGF-β1 and α2 (I) collagen cause the attenuated skin fibrosis in ET-$1^{f/f}$; Tie-2-Cre (+) mice.

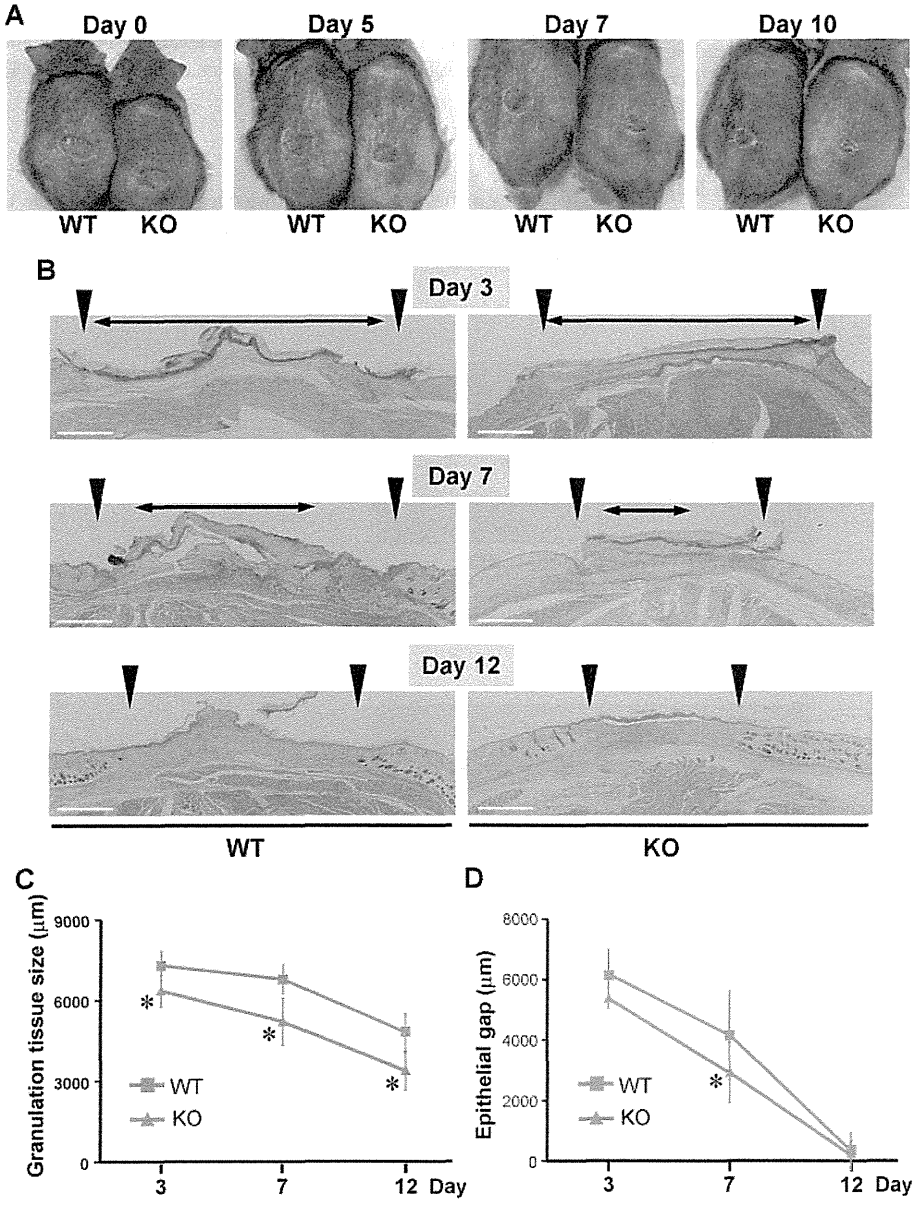

Figure 5. Cutaneous wound healing in WT and ET-$1^{f/f}$; Tie-2-Cre (+) mice. (A) Representative wound closure in wild-type (WT) and ET-$1^{f/f}$; Tie-2-Cre (+) (KO) mice at days 0, 5, 7, 10 post-wounding. (B) Hematoxylin-Eosin (HE) staining of wound tissues derived from wild-type (WT) and ET-$1^{f/f}$; Tie-2-Cre (+) (KO) mice at days 3, 7, 12 post-wounding. Arrow heads indicated bilateral edges of wound granulation tissue. Double-headed arrows indicated the distance between the leading edges of wounded epidermis. The one representative result is shown. Scale bar = 1000 μm. (C) Measurements of granulation tissue size (the distance between the arrow heads) in the wild-type (WT) and ET-$1^{f/f}$; Tie-2-Cre (+) (KO) mice at days 3, 7, 12 post-wounding. Data are expressed as the mean ± SD of six independent experiments. *$P<0.05$ as compared with the value in WT mice. (D) Measurements of epithelial gap (the distance of double-headed arrows) in the wild-type (WT) and ET-$1^{f/f}$; Tie-2-Cre (+) (KO) mice at days 3, 7, 12 post-wounding. Data are expressed as the mean ± SD of six independent experiments. *$P<0.05$ as compared with the value in WT mice.
doi:10.1371/journal.pone.0097972.g005

Wound closure, granulation tissue formation, and re-epithelialization in ET-1$^{f/f}$; Tie-2-Cre (+) mice

Next, we investigate the role of vascular endothelial cell-derived ET-1 in cutaneous wound repair. A full-thickness 8 mm excisional wound was made in the dorsal skin of ET-1$^{f/f}$; Tie-2-Cre (+) and WT mice, and they were examined for up to 12 days after wounded. In macroscopically, ET-1$^{f/f}$; Tie-2-Cre (+) mice showed enhanced wound healing than WT mice (Fig. 5A).

Then, wound and surrounding tissue were collected at days 3, 7 and 12 post-wounding, and were used to evaluate granulation tissue area (the distance between bilateral edges of granulation tissue consisted of newly formed capillaries, fibroblasts and macrophages) and epithelial gap (the distance between the leading edges of wounded epidermis) in HE stained section (Fig. 5B). The granulation tissue area was significantly smaller in ET-1$^{f/f}$; Tie-2-Cre (+) mice than in WT mice at day 3, which continued till day 12 (Fig. 5C). Similarly, the epithelial gap was significantly shorter in ET-1$^{f/f}$; Tie-2-Cre (+) mice than in WT mice at days 7 (Fig. 5D). Thus, the accelerating wound closure in ET-1$^{f/f}$; Tie-2-Cre (+) mice was also confirmed microscopically.

When the myeloperoxidase-positive neutrophils, F4/80-positive macrophages, or CD3-positive T cells were counted by immunostaining, the number of these cells tended to be slightly decreased in the wounding bed at days 3, 7, and 12 in ET-1$^{f/f}$; Tie-2-Cre (+) mice (Fig. 6A-C), but not statistically significant.

In addition, we compared the expression of ECM molecules in the wounding bed between these mice by quantitative real-time PCR (Fig. 7). At day 3 after wounding, ET-1$^{f/f}$; Tie-2-Cre (+) mice skin showed significantly decreased mRNA levels of TNF-α relative to WT mice. Furthermore, at day 7 after wounding, the mRNA levels of TNF-α, TGF-β1, CTGF, and α2 (I) collagen were down-regulated in ET-1$^{f/f}$; Tie-2-Cre (+) mice in comparison with those in WT mice. The decreased mRNA levels of TGF-β1 and α2 (I) collagen in ET-1$^{f/f}$; Tie-2-Cre (+) mice continued till day 12 after wounding.

Discussion

This study is the first, to our knowledge, to report the role of endothelial ET-1 in skin fibrosis and wound repair via regulating the expression of cytokines and ECM, using *in vivo* model.

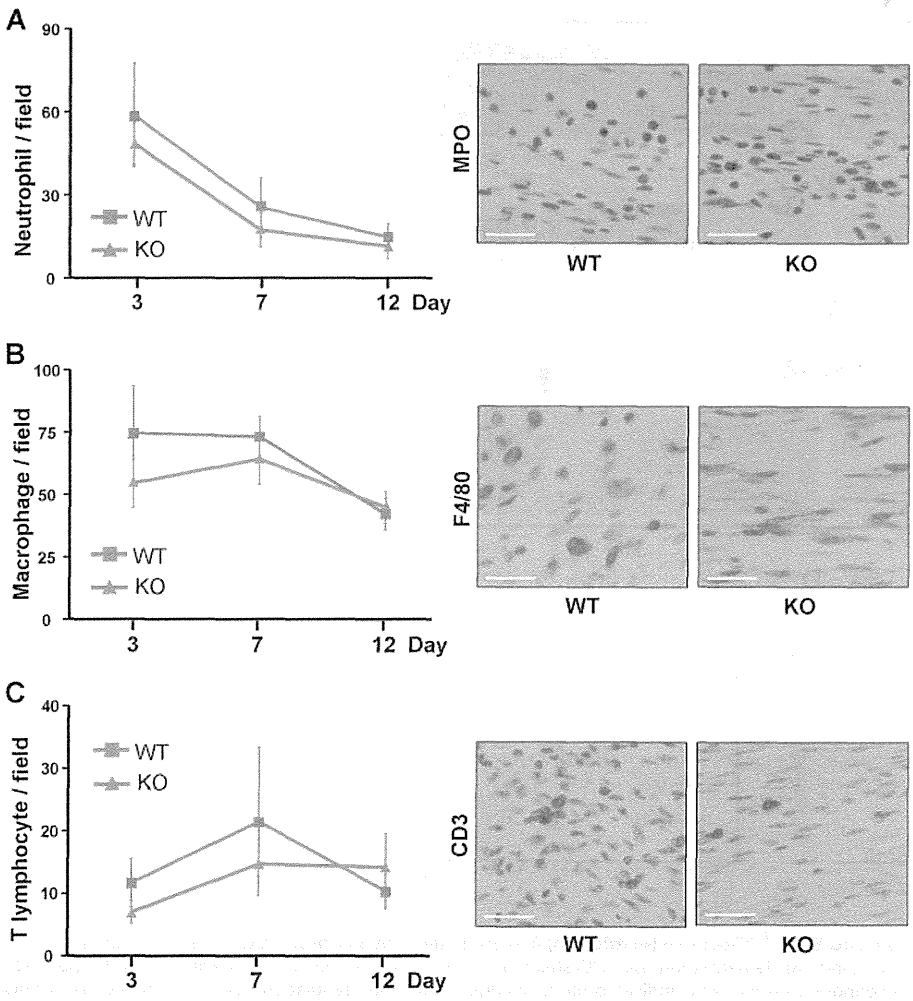

Figure 6. Infiltrating cells in the wounding bed at day 3, 7 and 12 of the wild-type (WT) and ET-1$^{f/f}$; Tie-2-Cre (+) (KO) mice. Myeloperoxidase (A), F4/80 (B) and CD3 (C) were stained. Positive cells were counted in five random high-power fields (0.06 mm^2, magnification, ×400). Data were expressed as the mean ± SD of six independent counts (left panel). The representative results of immunostaining for myeloperoxidase, F4/80 and CD3 are shown (right panel).
doi:10.1371/journal.pone.0097972.g006

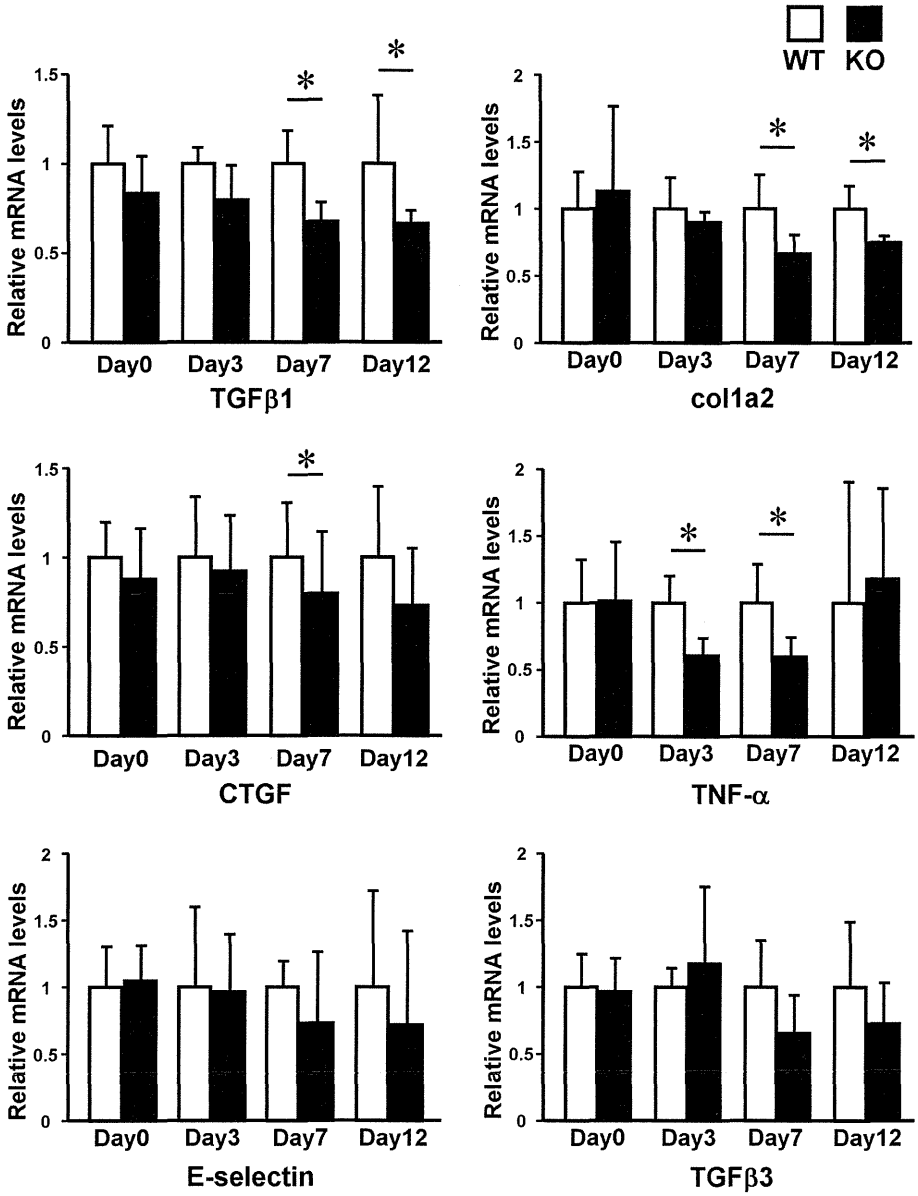

Figure 7. Cytokine expression in the wounding bed at day 3, 7 and 12 of the wild-type (WT) and ET-1$^{f/f}$; Tie-2-Cre (+) (KO) mice. Total RNA was extracted from the skin, and the mRNA expression levels of indicated cytokines were determined by real-time PCR. Data are expressed as the mean ± SD of six independent experiments. *$P<0.05$ as compared with the value in WT mice (1.0).
doi:10.1371/journal.pone.0097972.g007

The skin fibrosis induced by bleomycin injection in mice is known for a murine model of systemic sclerosis [14,19]. In this mouse model, inflammation cell such as T cells and macrophages are seen in the fibrotic lesion [20]. In addition, the development of bleomycin-induced skin fibrosis is accompanied by evidence of activation of TGF-β signaling [20]. We demonstrated that bleomycin-induced skin fibrosis was inhibited in endothelial cell-specific ET-1 knockout mice. Furthermore, we showed that the mRNA levels of TGF-β and α2 (I) collagen were decreased in bleomycin-treated skin of ET-1 knockout mice. On the other hand, there were no apparent differences in the number of inflammatory cells between endothelial ET-1 knockout mice and WT mice. Accordingly, the attenuated skin fibrosis in endothelial ET-1 knockout mice is likely to result from the lower TGF-β levels and subsequent lower collagen expression. Although previous studies have shown that ET-1 expression is potently regulated by TGF-β in endothelial cells and fibroblasts [21–23], our study first demonstrated ET-1 can also regulate TGF-β expression *in vivo*.

In the current study, we also observed that cutaneous wound healing in endothelial cell-specific ET-1 knockout mice was accelerated than in WT mice. Wound healing in the skin is a complex process including inflammation phase, new tissue formation phase, and tissue remodeling phase [24]. The interactions among the blood vessels, epidermis, leukocytes, dermal fibroblasts, ECM, various growth factors and cytokines are involved in each phase through controlling the replacement of granulation tissue by collagenous tissue and re-epithelialization [25,26]. The earlier reduction of granulation tissue and increased

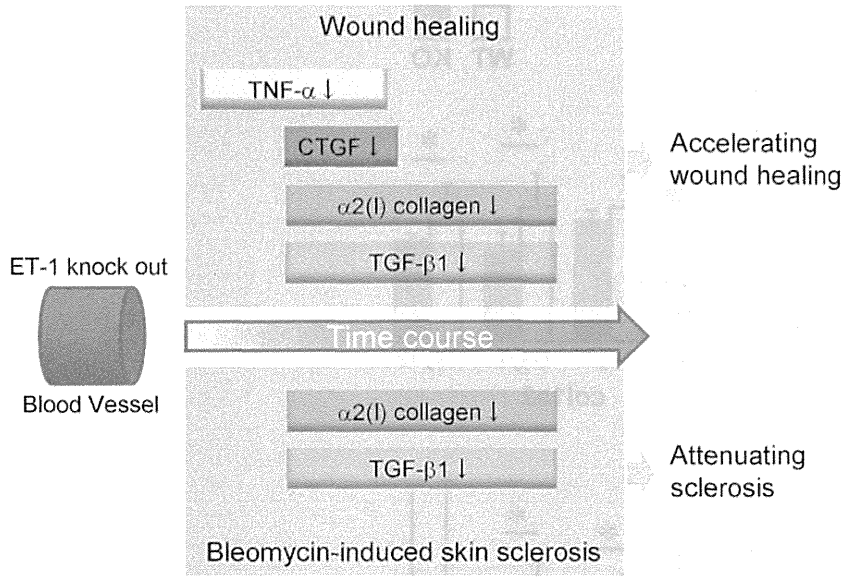

Figure 8. Schematic model of attenuated bleomycin-induced skin fibrosis and accelerated wound healing in endothelial cell-specific endothelin 1 knockout mice.
doi:10.1371/journal.pone.0097972.g008

re-epithelialization were seen in ET-1 knockout mice. However, there were no significant differences in inflammatory cell numbers between endothelial ET-1 knockout mouse and WT mice. On the other hand, the mRNA level of TNF-α, a proinflammatory cytokine, was significantly lower in early wound tissue of endothelial ET-1 knockout mice than that of WT mice. According to the previous literatures, the inhibition of TNF-α may have therapeutic value for refractory wound [27]. For example, wound healing in mouse is impaired by TNF-α up-regulation via the dysregulated inflammation and apoptosis [28]. Wound healing in TNF-α receptor-deficient mice was accelerated by reducing leukocyte infiltration [29]. Hence, the lower level of TNF-α in early wound of endothelial ET-1 knockout mouse may be one of the mechanisms for accelerating wound healing via affecting inflammatory phase. On the other hand, as seen in bleomycin-induced fibrosis model, the mRNA levels of TGF-β as well as α2 (I) collagen and CTGF were reduced in the wound of endothelial ET-1 knockout mice. Although TGF-β is an inducer of fibrosis via the synthesis of collagen and CTGF, previous studies have demonstrated that TGF-β may express adverse effects on the wound healing [30–34]. Furthermore, it is known that the early-gestation fetus has the prominent ability to cure skin wounds earlier without scarring, due to the lower levels of TGF-β [35,36]. Thus, reduced TGF-β expression may be another cause of the early would healing in endothelial ET-1 knockout mice.

Based on above findings, our hypothetical model of the role of vascular endothelial ET-1 in skin fibrosis and wound healing is shown in Fig. 8. In endothelial ET-1 knockout mouse, the expression of TNF-α, CTGF, TGF-β and collagen was down-regulated. As described in Introduction, bosentan attenuates skin fibrosis and accelerates wound healing in systemic sclerosis, and such contradictory effect may be mediated by above molecules. The endothelial cell-derived ET-1 is the potent therapeutic target in fibrosis or wound healing, and investigations of the overall regulatory mechanisms of these pathological conditions by ET-1 may lead to a new therapeutic approach.

There are several limitations in this study. First, because our main focus is to investigate whether ET-1 itself, rather than its receptors, are involved in the process of fibrosis or wound heal, we did not investigate the effect of bosentan or the contribution of each receptor in our mice model. In addition, although statistically significant, data related to gene expression was not dramatic. Future studies are needed to address these points.

Acknowledgments

The authors thank Mr. Keitaro Yamane and Ms. Chiemi Shiotsu for their valuable technical assistance; Ms. Michiyo Nakata and Prof. Yuichi Oike (Department of Molecular Genetics, Kumamoto University) for their assistance with Immunohistochemical staining; Dr. Yoshinobu Okamoto, Dr. Chihiro Tanaka and Dr. Manabu Fujimoto (Department of Dermatology, Kanazawa University) for their assistance with mice wound healing experiment.

Author Contributions

Conceived and designed the experiments: KM MJ HI. Performed the experiments: KM MJ TM. Analyzed the data: KM MJ JA IK SF KS. Contributed reagents/materials/analysis tools: KN NE MY. Wrote the paper: KM MJ.

References

1. Barton M, Yanagisawa M (2008) Endothelin: 20 years from discovery to therapy. Can J Physiol Pharmacol 86: 485–498.
2. Inoue A, Yanagisawa M, Kimura S, Kasuya Y, Miyauchi T, et al. (1989) The human endothelin family: three structurally and pharmacologically distinct isopeptides predicted by three separate genes. Proc Natl Acad Sci U S A 86: 2863–2867.
3. Watts S (2010) Endothelin receptors: what's new and what do we need to know? Am J Physiol Regul Integr Comp Physiol 298: R254–260.
4. Sauter G, Wolf S, Risler T, Brehm B (2004) Influence of endothelin receptor antagonism on smooth muscle cell proliferation after chronic renal failure. J Cardiovasc Pharmacol 44 Suppl 1: S165–167.
5. Komuro I, Kurihara H, Sugiyama T, Yoshizumi M, Takaku F, et al. (1988) Endothelin stimulates c-fos and c-myc expression and proliferation of vascular smooth muscle cells. FEBS Lett 238: 249–252.
6. Nishida M, Onohara N, Sato Y, Suda R, Ogushi M, et al. (2007) Galpha12/13-mediated up-regulation of TRPC6 negatively regulates endothelin-1-induced

cardiac myofibroblast formation and collagen synthesis through nuclear factor of activated T cells activation. J Biol Chem 282: 23117–23128.
7. Peng H, Carretero OA, Peterson EL, Yang XP, Santra K, et al. (2012) N-Acetyl-seryl-aspartyl-lysyl-proline inhibits ET-1-induced collagen production by preserving Src homology 2-containing protein tyrosine phosphatase-2 activity in cardiac fibroblasts. Pflugers Arch 464: 415–423.
8. Simonson MS, Ismail-Beigi F (2011) Endothelin-1 increases collagen accumulation in renal mesangial cells by stimulating a chemokine and cytokine autocrine signaling loop. J Biol Chem 286: 11003–11008.
9. Matucci-Cerinic M, Denton CP, Furst DE, Mayes MD, Hsu VM, et al. (2011) Bosentan treatment of digital ulcers related to systemic sclerosis: results from the RAPIDS-2 randomised, double-blind, placebo-controlled trial. Ann Rheum Dis 70: 32–38.
10. Giordano N, Puccetti L, Papakostas P, Di Pietra N, Bruni F, et al. (2010) Bosentan treatment for Raynauds phenomenon and skin fibrosis in patients with Systemic Sclerosis and pulmonary arterial hypertension: an open-label, observational, retrospective study. Int J Immunopathol Pharmacol 23: 1185–1194.
11. Kurihara Y, Kurihara H, Suzuki H, Kodama T, Maemura K, et al. (1994) Elevated blood pressure and craniofacial abnormalities in mice deficient in endothelin-1. Nature 368: 703–710.
12. Kisanuki Y, Emoto N, Ohuchi T, Widyantoro B, Yagi K, et al. (2010) Low blood pressure in endothelial cell-specific endothelin 1 knockout mice. Hypertension 56: 121–128.
13. Anggrahini D, Emoto N, Nakayama K, Widyantoro B, Adiarto S, et al. (2009) Vascular endothelial cell-derived endothelin-1 mediates vascular inflammation and neointima formation following blood flow cessation. Cardiovasc Res 82: 143–151.
14. Yamamoto T, Takagawa S, Katayama I, Yamazaki K, Hamazaki Y, et al. (1999) Animal model of sclerotic skin. I: Local injections of bleomycin induce sclerotic skin mimicking scleroderma. J Invest Dermatol 112: 456–462.
15. Tanaka C, Fujimoto M, Hamaguchi Y, Sato S, Takehara K, et al. (2010) Inducible costimulator ligand regulates bleomycin-induced lung and skin fibrosis in a mouse model independently of the inducible costimulator/inducible costimulator ligand pathway. Arthritis Rheum 62: 1723–1732.
16. Rho SS, Choi HJ, Min JK, Lee HW, Park H, et al. (2011) Clec14a is specifically expressed in endothelial cells and mediates cell to cell adhesion. Biochem Biophys Res Commun 404: 103–108.
17. Ernst C, Christie BR (2006) Isolectin-IB 4 as a vascular stain for the study of adult neurogenesis. J Neurosci Methods 150: 138–142.
18. Lopez-De Leon A, Rojkind M (1985) A simple micromethod for collagen and total protein determination in formalin-fixed paraffin-embedded sections. J Histochem Cytochem 33: 737–743.
19. Yamamoto T, Kuroda M, Nishioka K (2000) Animal model of sclerotic skin. III: Histopathological comparison of bleomycin-induced scleroderma in various mice strains. Arch Dermatol Res 292: 535–541.
20. Yamamoto T (2006) The bleomycin-induced scleroderma model: what have we learned for scleroderma pathogenesis? Arch Dermatol Res 297: 333–344.
21. Rodríguez-Pascual F, Redondo-Horcajo M, Lamas S (2003) Functional cooperation between Smad proteins and activator protein-1 regulates transforming growth factor-β-mediated induction of endothelin-1 expression. Circ Res 92: 1288–1295.
22. Horstmeyer A, Licht C, Scherr G, Eckes B, Krieg T (2005) Signalling and regulation of collagen I synthesis by ET-1 and TGF-β1. FEBS J 272: 6297–6309.
23. Shi-wen X, Kennedy L, Renzoni E, Bou-Gharios G, du Bois R, et al. (2007) Endothelin is a downstream mediator of profibrotic responses to transforming growth factor β in human lung fibroblasts. Arthritis Rheum 56: 4189–4194.
24. Gurtner G, Werner S, Barrandon Y, Longaker M (2008) Wound repair and regeneration. Nature 453: 314–321.
25. Singer A, Clark R (1999) Cutaneous wound healing. N Engl J Med 341: 738–746.
26. Martin P (1997) Wound healing—aiming for perfect skin regeneration. Science 276: 75–81.
27. Ashcroft GS, Jeong MJ, Ashworth JJ, Hardman M, Jin W, et al. (2012) Tumor necrosis factor-α (TNF-α) is a therapeutic target for impaired cutaneous wound healing. Wound Repair Regen 20: 38–49.
28. Siqueira MF, Li J, Chehab L, Desta T, Chino T, et al. (2010) Impaired wound healing in mouse models of diabetes is mediated by TNF-α dysregulation and associated with enhanced activation of forkhead box O1 (FOXO1). Diabetologia 53: 378–388.
29. Mori R, Kondo T, Ohshima T, Ishida Y, Mukaida N (2002) Accelerated wound healing in tumor necrosis factor receptor p55-deficient mice with reduced leukocyte infiltration. FASEB J 16: 963–974.
30. Shah M, Foreman DM, Ferguson MW (1994) Neutralising antibody to TGF-β 1,2 reduces cutaneous scarring in adult rodents. J Cell Sci 107 (Pt 5): 1137–1157.
31. Koch R, Roche N, Parks W, Ashcroft G, Letterio J, et al. (2000) Incisional wound healing in transforming growth factor-β1 null mice. Wound Repair Regen 8: 179–191.
32. Border WA, Ruoslahti E (1992) Transforming growth factor-β in disease: the dark side of tissue repair. J Clin Invest 90: 1–7.
33. Avraham T, Daluvoy S, Zampell J, Yan A, Haviv YS, et al. (2010) Blockade of transforming growth factor-β1 accelerates lymphatic regeneration during wound repair. Am J Pathol 177: 3202–3214.
34. Han G, Li F, Ten Dijke P, Wang XJ (2011) Temporal smad7 transgene induction in mouse epidermis accelerates skin wound healing. Am J Pathol 179: 1768–1779.
35. Bullard K, Longaker M, Lorenz H (2003) Fetal wound healing: current biology. World J Surg 27: 54–61.
36. Ferguson MW, O'Kane S (2004) Scar-free healing: from embryonic mechanisms to adult therapeutic intervention. Philos Trans R Soc Lond B Biol Sci 359: 839–850.

ARTHRITIS & RHEUMATOLOGY
Vol. 66, No. 6, June 2014, pp 1636–1647
DOI 10.1002/art.38380

Decreased Interleukin-20 Expression in Scleroderma Skin Contributes to Cutaneous Fibrosis

Hideo Kudo,[1] Masatoshi Jinnin,[1] Yoshihide Asano,[2] Maria Trojanowska,[3] Wakana Nakayama,[1] Kuniko Inoue,[1] Noritoshi Honda,[1] Ikko Kajihara,[1] Katsunari Makino,[1] Satoshi Fukushima,[1] and Hironobu Ihn[1]

Objective. **To clarify the role of interleukin-20 (IL-20) in the regulatory mechanism of extracellular matrix expression and to determine the contribution of IL-20 to the phenotype of systemic sclerosis (SSc).**

Methods. **Protein and messenger RNA (mRNA) levels of collagen, Fli-1, IL-20, and IL-20 receptor (IL-20R) were analyzed using polymerase chain reaction (PCR) array, immunoblotting, immunohistochemical staining, enzyme-linked immunosorbent assay, and real-time PCR.**

Results. **PCR array revealed that IL-20 decreased gene expression of α2(I) collagen (0.03-fold), Smad3 (0.02-fold), and endoglin (0.05-fold) in cultured normal dermal fibroblasts. Fli-1 protein expression was induced by IL-20 (~2-fold). The inhibition of collagen by IL-20, the induction of Fli-1 by IL-20, and the reduction of Smad3 and endoglin by IL-20 were also observed in SSc fibroblasts. Serum IL-20 levels were reduced only slightly in SSc patients but were significantly decreased in patients with scleroderma spectrum disorders (the prodromal stage of SSc) compared with those in normal subjects (111.3 pg/ml versus 180.4 pg/ml; $P < 0.05$). On the other hand, IL-20 mRNA expression in SSc skin was decreased compared with that in normal skin ($P < 0.05$), which may result in the induction of collagen synthesis in SSc dermal fibroblasts. IL-20R was expressed in normal and SSc fibroblasts. Moreover, IL-20 supplementation by injection into the skin reversed skin fibrosis induced by bleomycin in mice (~0.5-fold).**

Conclusion. **IL-20 reduces basal collagen transcription via Fli-1 induction, while down-regulation of Smad3 and endoglin may cancel the effect of transforming growth factor β in SSc fibroblasts. To confirm the therapeutic value of IL-20 and IL-20R, their function and expression in vivo should be further studied.**

Systemic sclerosis (SSc) or scleroderma is one of the rheumatic diseases characterized by tissue fibrosis of the skin and internal organs. In the skin, thickened dermis due to uncontrolled excessive deposition of extracellular matrix (ECM), mainly type I collagen (which consists of α1[I] and α2[I] collagen), is a hallmark of this disease (1,2). The source of the increased ECM is thought to be dermal fibroblasts activated by interactions with endothelial cells, lymphocytes, or macrophages, via various mediators including cytokines and growth factors (3,4). For example, many researchers have suggested that transforming growth factor β1 (TGFβ1) may play a central role in fibroblast activation (5–7). In addition, connective tissue growth factor (7), platelet-derived growth factor (8), insulin-like growth factor, interleukin-1 (IL-1), IL-6, and IL-7 are reported to be involved in the pathogenesis of this disease (9–12). Accordingly, investigating the cytokine network mediating fibroblast activation of SSc is essential to understand the molecular mechanism(s) of this disease.

IL-20 is identified as a member of the IL-10 family (13), which includes IL-10, IL-19, IL-22, IL-24 (melanoma differentiation–associated protein 7), and IL-26 (AK155). Although IL-19, IL-20, and IL-24 have partial homology in their amino acid sequences and share their receptor (14), the main biologic effects of these 3 cytokines seem quite distinct. IL-19 and IL-24 are mainly implicated in immune activity and tumor

[1]Hideo Kudo, MD, Masatoshi Jinnin, MD, PhD, Wakana Nakayama, MD, PhD, Kuniko Inoue, MD, PhD, Noritoshi Honda, MD, PhD, Ikko Kajihara, MD, PhD, Katsunari Makino, MD, PhD, Satoshi Fukushima, MD, PhD, Hironobu Ihn, MD, PhD: Kumamoto University, Kumamoto, Japan; [2]Yoshihide Asano, MD, PhD: University of Tokyo Graduate School of Medicine, Tokyo, Japan; [3]Maria Trojanowska, MD, PhD: Boston University School of Medicine, Boston, Massachusetts.

Address correspondence to Masatoshi Jinnin, MD, PhD, Department of Dermatology and Plastic Surgery, Faculty of Life Sciences, Kumamoto University, Honjo 1-1-1, Kumamoto 860-8556, Japan. E-mail: mjin@kumamoto-u.ac.jp.

Submitted for publication May 4, 2013; accepted in revised form January 21, 2014.

apoptosis, respectively (15–17). On the other hand, IL-20 is expressed by multiple cell types, including monocytes and skin keratinocytes, and is implicated in the pathogenesis of autoimmune diseases. IL-20 was reportedly elevated in synovial fluid from patients with rheumatoid arthritis (18). Moreover, IL-20 is thought to be correlated with the etiology of lupus nephritis (19,20). In addition, IL-20 expression and IL-20 receptor (IL-20R) complexes are dramatically up-regulated in psoriatic skin lesions (21). However, there have been no reports that validate the function of IL-20 in the regulation of ECM or the pathogenesis of SSc.

In the present study, we investigated the effect of IL-20 on ECM expression in normal fibroblasts. In addition, we compared the expression pattern of IL-20 in the sera and skin between normal subjects and SSc patients, and we demonstrated the involvement of IL-20 signaling in the abnormal ECM regulation seen in SSc.

PATIENTS AND METHODS

Reagents. Recombinant human IL-19, IL-20, and IL-24 and mouse IL-20 were obtained from R&D Systems.

Patients. Serum samples were obtained from 33 patients with SSc (5 males and 28 females, mean age 58.7 years [range 24–85 years]); 13 had diffuse cutaneous SSc (dcSSc), and 20 had limited cutaneous SSc. All patients fulfilled the classification criteria proposed by the American College of Rheumatology (ACR) (22). We also included in the study 10 patients with systemic lupus erythematosus (SLE), 12 patients with dermatomyositis (DM), and 9 patients with scleroderma spectrum disorders who did not fulfill the ACR classification criteria for SSc but who we thought would meet these criteria in the future (23–25) (further information available from the corresponding author). Control serum samples were also obtained from 15 healthy volunteers. Skin biopsy specimens of lesional skin were obtained from SSc patients. Control samples of routinely discarded skin were obtained from healthy human subjects undergoing skin grafts. Institutional review board approval and written informed consent according to the Declaration of Helsinki were obtained before patients and healthy volunteers were entered into this study.

Diagnosis of scleroderma spectrum disorders by the point system. A total score was evaluated as the sum of 5 factors for the diagnosis of scleroderma spectrum disorders (23–25):

1. Skin sclerosis: swollen fingers = 1 point, sclerodactyly = 3 points, proximal sclerosis = 5 points, diffuse sclerosis = 10 points.
2. Pulmonary changes: pulmonary fibrosis accompanied by forced vital capacity (FVC) ≥80% predicted = 2 points, pulmonary fibrosis accompanied by FVC <80% predicted = 4 points.
3. Antinuclear antibodies (ANAs): anti–topoisomerase I antibody = 5 points, anticentromere or anti–U1 RNP antibody = 3 points, antinucleolar antibody = 2 points, other ANAs = 1 point.
4. Pattern of Raynaud's phenomenon: biphasic or bilateral = 1 point, biphasic and bilateral = 2 points, triphasic = 3 points.
5. Nailfold bleeding: 1 or 2 fingers = 1 point, ≥3 fingers = 2 points.

A total score of 5–8 is consistent with scleroderma spectrum disorders, and a total score of ≥9 is consistent with SSc.

Cell cultures. Human dermal fibroblasts were obtained by skin biopsies of the affected areas (dorsal forearm) of 7 healthy human subjects and dcSSc patients (26). Institutional review board approval and written informed consent were obtained according to the Declaration of Helsinki. Independently isolated monolayer cultures of fibroblasts obtained from different individuals were maintained at 37°C in 5% CO_2 in air. Cells were serum-starved for 24 hours before all experiments.

Cell lysis and immunoblotting. Cultured fibroblasts were washed twice with cold phosphate buffered saline (PBS) and lysed in Denaturing Cell Extraction Buffer (BioSource International). Aliquots of the cell lysates (normalized for protein concentrations) were separated by electrophoresis on 10% sodium dodecyl sulfate–polyacrylamide gels and transferred onto PVDF filters. The PVDF filters were then incubated with antibodies against type I collagen (SouthernBiotech) or against Ets-1, Fli-1, IL-20R, or β-actin (all from Santa Cruz Biotechnology). The filters were incubated with secondary antibody, and the immunoreactive bands were visualized using an ECL system (Amersham Biosciences).

Immunohistochemistry. Wax-embedded sections (4-μm thickness) were dewaxed in xylene and rehydrated in graded alcohols. For the immunostaining of IL-20 and Smad3, antigens were retrieved by incubation with citrate buffer (pH 6) for 9 minutes with a microwave. Endogenous peroxidase activity was inhibited with a solution of 0.3% H_2O_2 in methyl alcohol, after which sections were blocked with 5% donkey serum for 20 minutes and then reacted with antibodies to IL-20 (Abcam) or Smad3 (Santa Cruz Biotechnology) at 4°C. After excess antibody was washed out with PBS, samples were incubated with horseradish peroxidase (HRP)–labeled anti-mouse antibody (Nichirei Biosciences) at 37°C.

For immunostaining of IL-20R or Fli-1, antigens were retrieved by incubation with citrate buffer (pH 9) for 9 minutes with a microwave. Antibodies to IL-20R (Abcam) and Fli-1 (Santa Cruz Biotechnology) and HRP-labeled anti-rabbit antibody (Nichirei Biosciences) were used.

The reaction was visualized using a diaminobenzidine substrate system (Dojin). Slides were counterstained with Mayer's hematoxylin and examined under a light microscope (BX50; Olympus).

RNA isolation, array analysis, and quantitative real-time polymerase chain reaction (PCR). Total RNA was extracted from culture cells with Isogen (Nippon Gene) or from paraffin-embedded sections with an RNeasy FFPE kit (Qiagen). For the array, first-strand complementary DNA (cDNA) was synthesized from RNA using an RT^2 First Strand Kit (Qiagen). Complementary DNA was mixed with RT^2 SYBR Green/Rox qPCR Master Mix (Qiagen), and the mixture was added to a 96-well Extracellular Matrix and Adhesion Molecules PCR Array (Qiagen). PCR was performed on a Takara Thermal Cycler Dice (TP800) instrument (Takara Bio). The threshold cycle (C_t) for each RNA was extracted using Ther-

mal Cycler Dice Real Time System software, version 2.10B (Takara Bio). The raw C_t was normalized using the values of housekeeping genes. For quantitative real-time PCR, first-strand cDNA was synthesized using a PrimeScript RT reagent Kit (Takara Bio) (27). GAPDH primer was purchased from Qiagen, and other primers were purchased from Takara Bio. Using a Takara Thermal Cycler Dice instrument, DNA was amplified for 40 cycles of denaturation for 5 seconds at 95°C and annealing for 30 seconds at 60°C. The relative expression of each gene of interest and GAPDH was calculated using a standard curve method.

Immunoprecipitation. Phosphorylated Fli-1 was detected as described previously (28). For the detection of acetylated Fli-1, cells were lysed in Pierce IP lysis buffer with the Halt phosphatase inhibitor cocktail (Thermo Scientific Pierce). Cell lysates were precleared with protein G–Sepharose (GE Healthcare) and then were incubated with monoclonal mouse anti–Fli-1 antibody (BD Biosciences) and protein G–Sepharose beads overnight at 4°C. The immunoprecipitated proteins were washed with Pierce buffer. Agarose-bound proteins were extracted by incubation in sample buffer at 95°C. The sample was then assessed by immunoblotting with anti–acetylated lysine antibody (Cell Signaling Technology). The membrane was stripped and reprobed with rabbit polyclonal anti–Fli-1 antibody (Santa Cruz Biotechnology) (29).

Chromatin immunoprecipitation (ChIP) assay. ChIP assay was performed using an EpiQuik ChIP kit (Epigentek) (28). Briefly, after cells were treated with 1% formaldehyde for 10 minutes, the crosslinked chromatin was sonicated. The DNA fragments were immunoprecipitated with IgG isotype control antibody or polyclonal anti–Fli-1 antibody at room temperature. After crosslinking was reversed, the immunoprecipitated chromatin was amplified by PCR of a specific region of the α2(I) collagen genomic locus. The primers used were 5′-CTGGACAGCTCCTGCTTTGAT-3′ (forward) and 5′-CTTTCAAGGGGAAACTCTGACTC-3′ (reverse). The amplified DNA products were run out on an agarose gel containing ethidium bromide.

Plasmid construction. A construct consisting of the full-length human α2(I) collagen gene fragment linked to the chloramphenicol acetyltransferase (CAT) reporter gene and a series of 5′-deletions of the construct were generated as previously described (30).

Transient transfection. For CAT assay, fibroblasts were transfected with promoter constructs employing Lipofectamine 2000 (Invitrogen), as described previously (30). In order to correct minor variations in transfection efficiency, pSV-β-galactosidase vector (Promega) was included in all transfections.

For reverse transfection of small interfering RNAs (siRNAs), siRNAs were mixed with Lipofectamine RNAiMAX (Invitrogen) and then added when the cells were plated, followed by incubation at 37°C in 5% CO_2. Small interfering RNA against Fli-1 and control siRNA were purchased from Dharmacon.

CAT assay. After 48 hours of incubation after the transfection of constructs with CAT reporter, cells were harvested. CAT activity in cell lysates was assayed colorimetrically using a CAT ELISA kit (Roche) (31).

Immunofluorescence microscopy. Fibroblasts were grown in 4-well LAB TEK chambers (Nunc) to subconfluence as described above. Immunofluorescence was performed using antibody to IL-20R as primary antibody and fluorescein isothiocyanate–conjugated donkey anti-goat IgG (Santa Cruz Biotechnology) as secondary antibody. A Zeiss fluorescence microscope was used (6) to visualize fluorescence.

Measurement of serum IL-20 concentrations. Serum IL-20 levels were measured with a specific enzyme-linked immunosorbent assay (ELISA) kit (Human IL-20 Immunoassay; R&D Systems) (27,32). Briefly, antibody to IL-20 was precoated onto microtiter wells. Aliquots of serum were added to each well, followed by peroxidase-conjugated antibodies to IL-20. Color was developed with H_2O_2 and tetramethylbenzidine peroxidase, and absorbance at 450 nm was measured. Wavelength correction was performed by absorbance at 540 nm. The concentration of IL-20 in each sample was determined by interpolation from a standard curve.

Intradermal treatment with bleomycin. Bleomycin (Nippon Kayaku) was dissolved in PBS at a concentration of 1 mg/ml and sterilized by filtration. Bleomycin (300 μg) or PBS was injected intradermally into the shaved backs of 6-week-old BALB/c mice 6 times per week for 1 month, as described previously (33,34). Injection was performed using a 27-gauge needle. The back skin was removed on the day after the final injection. The skin samples were then fixed in 10% formalin solution and embedded in paraffin. Sections were stained with hematoxylin and eosin (H&E). Dermal thickness was evaluated by 2 investigators (HK, WN) in a blinded manner who measured the distance between the epidermal–dermal junction and the dermal–fat junction in H&E-stained sections under 100× magnification.

Collagen assay. The amount of collagen in the paraffin-embedded skin sections was quantified using a Sircol Soluble Collagen Assay Kit (Chondrex). After being dewaxed in xylene and rehydrated in graded alcohols, 20-μm thick sections were immersed in staining solution at room temperature for 30 minutes. The staining solution was removed and a bleaching solution was added to measure the absorbance at 540 nm and 605 nm in an ND-1000 spectrophotometer (NanoDrop Technologies). The collagen concentration was calculated based on the following formula: collagen (μg/section) = (optical density [OD] at 540 nm – [$OD_{605} \times 0.291$])/37.8 × 1,000 (35).

Statistical analysis. Data presented as bar graphs are the mean ± SEM of at least 3 independent experiments. The statistical analysis was carried out using the Mann-Whitney U test for the comparison of medians and Fisher's exact probability test for the analysis of frequency. *P* values less than 0.05 were considered significant.

RESULTS

Effect of IL-20 on expression of ECM-related genes in cultured normal dermal fibroblasts. As an initial experiment, to determine the effect of IL-20 on ECM expression, we performed a PCR array of 84 ECM-related genes using RNA obtained from 3 dermal fibroblasts either unstimulated or stimulated with IL-20 for 12 hours. When a 16-fold difference by the $\Delta\Delta C_t$ method was considered meaningful, 3 of the 84 genes were up-regulated and 13 genes were down-regulated in

Table 1. Expression profiles of extracellular matrix–related genes in the presence or absence of IL-20 in the PCR array*

Gene symbol	Gene name	Fold change
Genes up-regulated by IL-20		
THBS2	Thrombospondin 2	113.77
TGIF1	TGFB-induced factor homeobox 1	57.28
MMP9	Matrix metallopeptidase 9	33.13
Genes down-regulated by IL-20		
MMP3	Matrix metallopeptidase 3	0.02
SERPINA1	Serpin peptidase inhibitor, clade A, member 1	0.02
SMAD3	SMAD family member 3	0.02
DCN	Decorin	0.03
PLAU	Plasminogen activator, urokinase	0.03
LOX	Lysyl oxidase	0.03
COL1A2	Collagen, type I, α2	0.03
ENG	Endoglin	0.05
CAV1	Caveolin 1, caveolae protein, 22 kd	0.05
IL5	Interleukin 5	0.06
FASLG	Fas ligand	0.06
IL10	Interleukin 10	0.06
IL1A	Interleukin 1, α	0.06

* A mixture of equal amounts of mRNAs from 3 normal fibroblasts was prepared in the presence or absence of interleukin-20 (IL-20), and the mRNA expression profile was evaluated using a polymerase chain reaction (PCR) array. Fold change was calculated as $1/2^{(\text{raw Ct of each mRNA} - \text{Ct of housekeeping genes})}$. Genes up- or down-regulated >16-fold by IL-20 stimulation are shown.

IL-20–treated fibroblasts in comparison with untreated cells (Table 1). Among them, human α2(I) collagen gene expression was decreased 0.03-fold by IL-20. Consistent with the array result, quantitative real-time PCR using specific primers for α1(I) or α2(I) collagen and an increased number of samples (n = 7) showed that collagen messenger RNA (mRNA) expression was significantly reduced by IL-20 (Figure 1A). Furthermore, immunoblotting revealed that the protein synthesis of type I collagen was also decreased in a dose-dependent manner by treatment with IL-20, and the decrease was statistically significant ($P < 0.05$) (Figure 1B).

To determine whether the down-regulation of collagen by IL-20 takes place at the transcriptional level or translational level, stability of collagen mRNA was examined. Because the steady-state level of mRNA is controlled by the level of gene transcription and/or the stability of mRNA, de novo mRNA synthesis was blocked by the RNA synthesis inhibitor actinomycin D in normal fibroblasts in the presence or absence of IL-20. As shown in Figure 1C, after actinomycin D treatment, there was no significant difference in the decrease rate of α2(I) collagen mRNA between cells with and those without IL-20. Similarly, when de novo protein synthesis and the expression of proteolytic enzymes were blocked with cycloheximide, IL-20 stimulation had little effect on the half-lives of collagen protein (Figure 1D). Taken together, these results indicate that the stability of collagen mRNA and protein was not altered by IL-20, and proteolytic enzymes were less likely to be involved in the effect of IL-20 on collagen expression. Thus, collagen synthesis is thought to be decreased by IL-20 at the transcriptional level.

Next, to identify the element of the human α2(I) collagen promoter that responds to IL-20 stimulation, we compared activities of serial 5′-deletions of the promoter linked to the CAT reporter gene in the presence or absence of IL-20 in normal fibroblasts (Figure 1E). The full-length −3500 to +58 bp construct and the shorter construct with deletion end points at −353 to +58 bp showed a similar fold decrease of promoter activities by IL-20 relative to the values in untreated fibroblasts (~0.3-fold). The −264 to +58 bp construct and shorter constructs did not respond to IL-20 stimulation, indicating that the element of the α2(I) collagen promoter gene that responds to IL-20 is located between −353 and −264 bp.

This region contains the binding sites for Sp1, Ets family transcription factors (e.g., Ets-1 and Fli-1), and CCAAT/enhancer binding protein β (c/EBPβ) (Figure 1E). According to the results of the PCR array, the expression of c/EBPβ and Sp1 was not affected by IL-20 (not shown). Real-time PCR showed that IL-20 induced the expression of Fli-1 but not that of Ets-1 (Figure 2A). In addition, the protein expression of Fli-1 was also increased by IL-20 (Figure 2B). Fli-1 is thought to share binding sites with Ets-1, and it inhibits α2(I) collagen promoter activity by competing with Ets-1 using an overexpression system in vitro (36,37), indicating that the balance of Ets-1 and Fli-1 controls collagen expression (36,38). We found that the ratio of Ets-1:Fli-1 protein expression was significantly decreased by IL-20. Several lines of evidence revealed that posttranslation modification, such as phosphorylation and acetylation, tightly regulates the protein stability and transcriptional activity of Fli-1 (29). Although both phosphorylation and acetylation of Fli-1 were not changed by IL-20 (Figure 2C), the cytokine increased the association of Fli-1 with the collagen promoter in chromatin immunoprecipitates (Figure 2D). These data indicate that IL-20 increased FIi-1 protein through the induction of Fli-1 mRNA levels directly without the alterations of phosphorylation and acetylation.

We also examined the mRNA expression of other human α2(I) collagen promoter–related molecules by real-time PCR. The expression of c-Myb, c-Fos, and

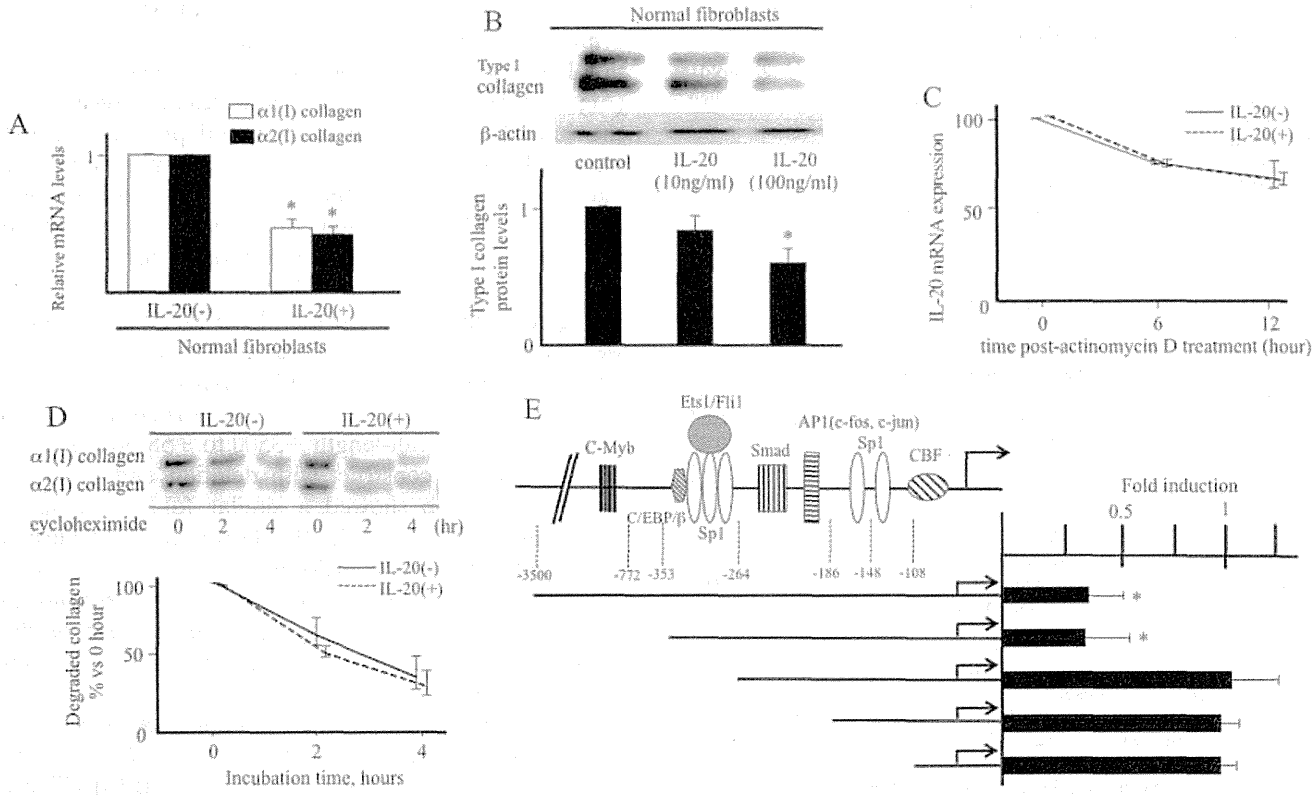

Figure 1. Effect of interleukin-20 (IL-20) on collagen expression. **A,** Normal fibroblasts were treated with IL-20 (100 ng/ml) for 12 hours. Levels of collagen mRNA were determined by real-time polymerase chain reaction (PCR) (n = 7 samples). * = $P < 0.05$ versus untreated fibroblasts (set to 1.0). **B,** Normal fibroblasts were treated with IL-20 (100 ng/ml) for 24 hours. Cell lysates were subjected to immunoblotting. The protein levels of type I collagen quantitated by scanning densitometry and corrected for the levels of β-actin in the same samples are shown relative to those in untreated fibroblasts (set to 1.0) (n = 3 samples). * = $P < 0.05$ versus untreated fibroblasts. **C,** Fibroblasts were incubated in the presence or absence of IL-20 for 12 hours before the addition of 2.5 μg/ml actinomycin D for 6 or 12 hours. IL-20 mRNA expression was analyzed by real-time PCR. **D,** Fibroblasts were incubated in the presence or absence of IL-20 for 24 hours before the addition of cycloheximide (10 μg/ml). Cells were harvested at the indicated time points after cycloheximide was administered, and immunoblotting was performed. The protein levels of type I collagen quantitated by scanning densitometry and corrected for the levels of β-actin in the same samples are shown relative to those in untreated fibroblasts (set to 1.0) (n = 3 samples). **E,** The indicated α2(I) collagen promoter deletion constructs were transfected into normal fibroblasts in the absence or presence of IL-20 (100 ng/ml) for 24 hours (n = 3 samples). The bar graph represents fold stimulation of chloramphenicol acetyltransferase activities stimulated with IL-20 relative to those not stimulated with IL-20 (set to 1.0). * = $P < 0.05$ versus cells not stimulated with IL-20. Values are the mean ± SEM. c/EBPβ = CCAAT/enhancer binding protein β; AP-1 = activator protein 1; CBF = CCAAT-binding transcription factor.

c-Jun was not affected by IL-20 (Figure 2A). Caveolin 1 was down-regulated by IL-20 in the array (Table 1), but the decrease became insignificant in real-time PCR with increasing the number of samples (n = 7) (Figure 2E). Smad3 and endoglin, mediators of TGFβ signaling, were significantly decreased by IL-20 (Figure 2E), consistent with the array results. However, the decrease of Smad3 or endoglin could not explain the reduction of α2(I) collagen expression by IL-20 in normal fibroblasts, because their inhibition was shown to have no effect on basal collagen transcription (39,40). Therefore, our results suggest that IL-20 reduces collagen transcription mainly via Fli-1 expression. Consistent with our hypothesis, the inhibitory effect of IL-20 on collagen was blocked by the transfection of Fli-1 siRNA (Figure 2F).

As described above, IL-19, IL-20, and IL-24 share a receptor (14), although their functions are different. We investigated whether IL-19 and IL-24 also regulate collagen expression in vitro. Immunoblotting revealed that protein synthesis of type I collagen was not significantly affected by treatment with IL-19 or IL-24 in comparison with untreated cells (further information available from the corresponding author). When the ratio of Ets-1:Fli-1 was also examined by immunoblotting, we did not find significant change (further information available from the corresponding author).

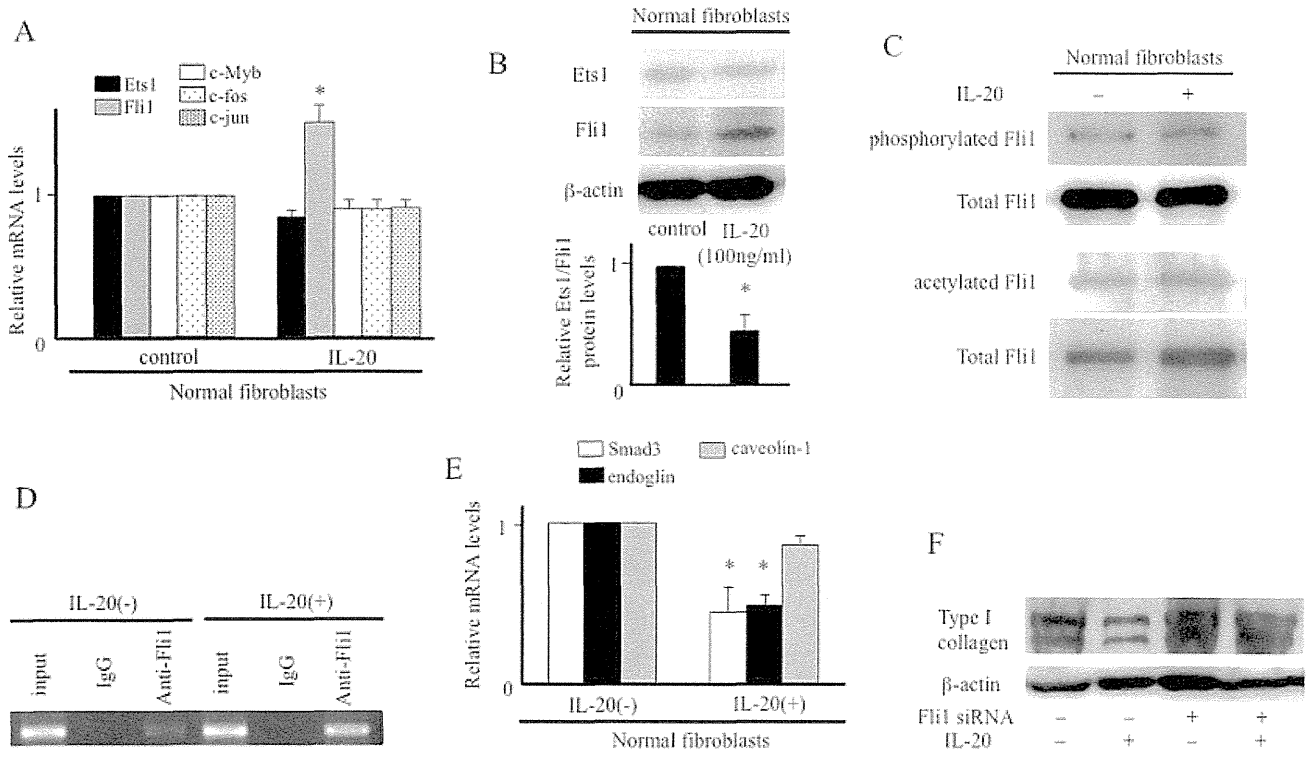

Figure 2. Effect of interleukin-20 (IL-20) on Fli-1 expression. **A,** Normal fibroblasts were incubated in the presence or absence of IL-20 for 12 hours. Messenger RNA levels were determined by real-time polymerase chain reaction (PCR) (n = 7 samples). * = $P < 0.05$ versus untreated fibroblasts (set to 1.0). **B,** Normal fibroblasts were treated with IL-20 for 24 hours. Immunoblotting was performed using antibody to Ets-1 or Fli-1. Protein levels of Ets-1 and Fli-1 were quantitated as described in Figure 1B, and the ratio of Ets-1:Fli-1 protein expression is shown. * = $P < 0.05$ versus untreated fibroblasts (set to 1.0) (n = 3 samples). **C,** Normal fibroblasts were treated with IL-20 (100 ng/ml) for 24 hours. Levels of phosphorylated and acetylated Fli-1 were determined as described in Patients and Methods. **D,** Normal fibroblasts were incubated in the presence or absence of IL-20 for 12 hours. Cellular DNA was sheared, and chromatin (input DNA) was immunoprecipitated with anti–Fli-1 antibody or IgG isotype control antibody. The presence of α2(I) collagen promoter fragments in the precipitates was detected using PCR followed by agarose gel electrophoresis. **E,** Levels of Smad3, endoglin, and caveolin 1 mRNA were determined as described in **A.** * = $P < 0.05$ versus untreated fibroblasts (set to 1.0) (n = 7 samples). **F,** Normal fibroblasts were treated with IL-20 (100 ng/ml) for 12 hours in the presence or absence of Fli-1 small interfering RNA (siRNA). The expression of type I collagen was determined by immunoblotting. Values are the mean ± SEM.

Therefore, among IL-20R–related cytokines, the reduction of collagen expression via Fli-1 up-regulation is likely to be specific to IL-20.

Expression levels of IL-20 in sera and involved skin of patients with SSc. Next, we measured the serum levels of IL-20 in various rheumatic diseases by ELISA. As shown in Figure 3A, the mean serum IL-20 levels in patients with SSc, SLE, and DM were slightly but not significantly decreased compared with those in normal subjects. On the other hand, patients with scleroderma spectrum disorders who did not fulfill the ACR classification criteria for SSc but who we thought would develop SSc in the future (23–25) had IL-20 levels significantly lower than those in normal subjects.

We determined the association of serum IL-20 levels with clinical features and laboratory findings in SSc patients (further information available from the corresponding author). Patients with decreased IL-20 levels (below the average of normal subjects) had a significantly higher prevalence of esophageal involvement than did those with normal IL-20 levels (52.9% versus 12.5%; $P < 0.05$). The modified Rodnan skin thickness score (41) was also increased, although not significantly, in those with decreased IL-20 levels. In contrast, as determined by real-time PCR, IL-20 mRNA expression in involved skin of SSc patients was significantly decreased compared with that in skin of normal subjects (Figure 3B). Immunohistochemical staining using paraffin-embedded skin sections also showed that IL-20 protein was detected strongly in the epidermis of normal skin but hardly detected in SSc atrophic epidermis (Figure 3C). Thus, serum IL-20 levels may be

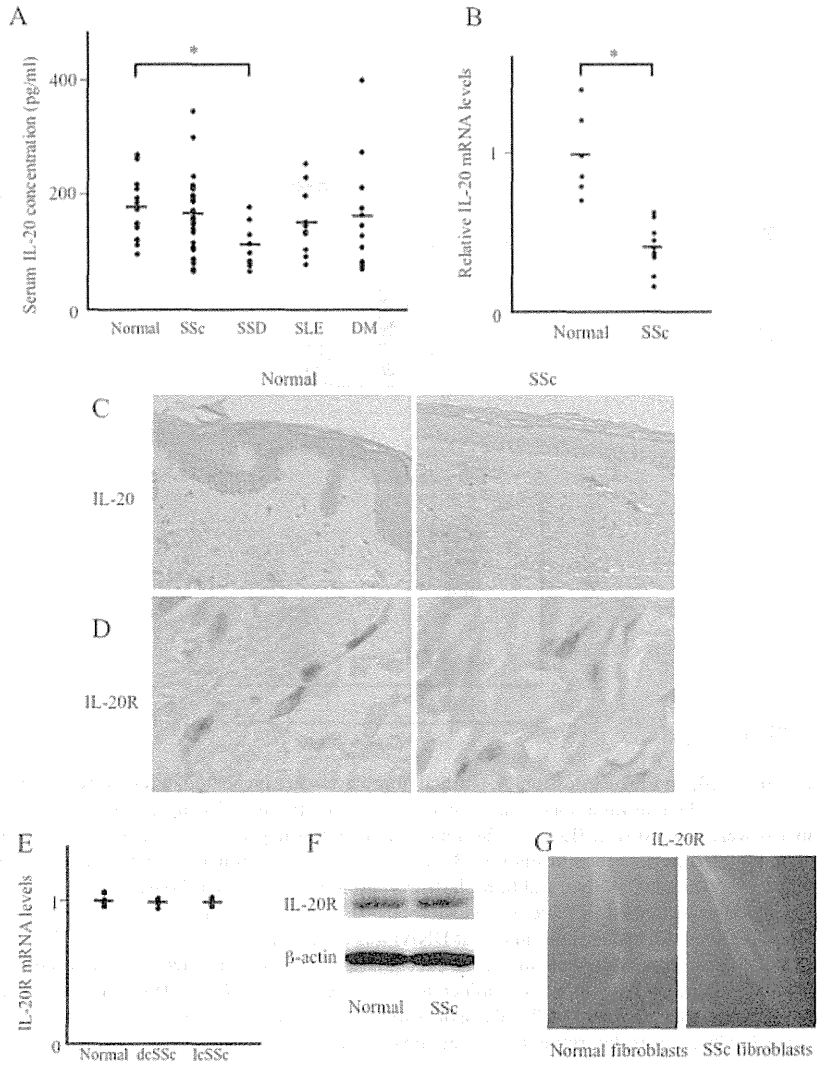

Figure 3. Interleukin-20 (IL-20) levels in sera and skin tissues from patients with rheumatic diseases. **A,** Shown are serum IL-20 levels as determined by enzyme-linked immunosorbent assay. Serum samples were obtained from 33 patients with systemic sclerosis (SSc), 9 patients with scleroderma spectrum disorders (SSD), 10 patients with systemic lupus erythematosus (SLE), 12 patients with dermatomyositis (DM), and 15 normal subjects. Symbols represent individual samples; bars show the mean. $* = P < 0.05$. **B,** Total RNA was extracted from skin tissues obtained from 12 SSc patients and 6 normal subjects. IL-20 mRNA expression was analyzed by real-time polymerase chain reaction (PCR). Symbols represent individual samples; bars show the mean. $* = P < 0.05$. **C,** Paraffin-embedded sections of normal and SSc-involved skin were subjected to immunohistochemical analysis for IL-20. Original magnification × 200 (n = 3 samples). **D,** Paraffin-embedded sections of normal and SSc-involved skin were subjected to immunohistochemical analysis for IL-20 receptor (IL-20R). Original magnification × 400 (n = 3 samples). **E,** Total RNA was extracted, and IL-20R mRNA expression was analyzed by real-time PCR as described in **B**. Symbols represent individual samples; bars show the mean. **F,** Cell lysates were obtained from cultured normal and SSc dermal fibroblasts and subjected to immunoblotting with antibody to IL-20R. Results are representative of 5 normal and 5 SSc fibroblasts. **G,** Expression of IL-20R in cultured normal dermal fibroblasts and SSc fibroblasts was visualized by immunofluorescence microscopy. Original magnification × 1,000. dcSSc = diffuse cutaneous SSc; lcSSc = limited cutaneous SSc.

specifically decreased in the prodromal stage of SSc, while IL-20 expression in involved skin of SSc patients may be constitutively decreased.

Although there has been no previous report indicating that IL-20R is expressed in dermal fibroblasts, immunostaining revealed that IL-20R protein was expressed to a similar extent in fibroblast-like spindle-shaped cells of normal and SSc skin in vivo (Figure 3D). This result was consistent with similar IL-20R expression levels in normal and SSc skin by real-time PCR in vivo

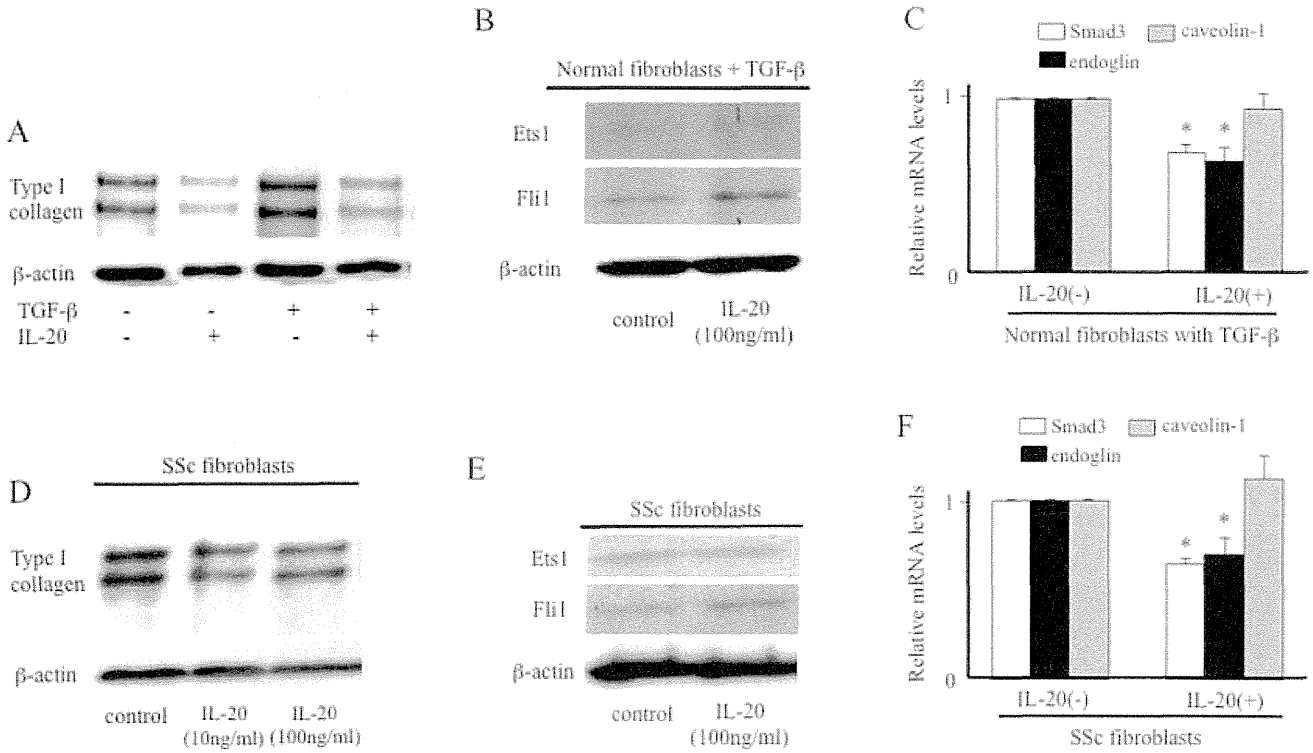

Figure 4. Effect of IL-20 on collagen expression in transforming growth factor β (TGFβ)–stimulated normal fibroblasts or SSc fibroblasts. **A,** Normal fibroblasts were treated with IL-20 (100 ng/ml) and/or TGFβ (2 ng/ml) for 24 hours. The expression of type I collagen was evaluated by immunoblotting. **B,** Normal fibroblasts were treated with IL-20 in the presence of TGFβ (2 ng/ml) for 24 hours. Immunoblotting was performed using antibody to Ets-1 or Fli-1. **C,** Normal fibroblasts were treated with IL-20 (100 ng/ml) for 12 hours in the presence of TGFβ (2 ng/ml). Real-time PCR was performed to evaluate levels of Smad3, endoglin, and caveolin 1 mRNA (n = 7 samples). * = $P < 0.05$ versus untreated fibroblasts (set to 1.0). **D,** SSc fibroblasts were treated with IL-20 for 24 hours. Immunoblotting was performed using antibody to type I collagen. **E,** SSc fibroblasts were treated with IL-20 for 24 hours. Immunoblotting was performed using antibody to Ets-1 or Fli-1. **F,** SSc fibroblasts were treated with IL-20 (100 ng/ml) for 12 hours. Real-time PCR was performed to evaluate levels of Smad3, endoglin, and caveolin 1 mRNA (n = 7 samples). * = $P < 0.05$ versus untreated fibroblasts (set to 1.0). Values are the mean ± SEM. See Figure 3 for other definitions.

(Figure 3E) or by immunoblotting (Figure 3F) and immunofluorescence (Figure 3G) in vitro using cultured fibroblasts. Thus, dermal fibroblasts may express IL-20R, and its expression levels are likely to be similar in normal and SSc fibroblasts. Taken together, these results indicate that IL-20 may have an inhibitory effect on collagen expression, and down-regulation of IL-20 levels in SSc skin in vivo contributes to increased collagen accumulation and tissue fibrosis.

Effect of IL-20 on type I collagen expression in TGFβ-stimulated normal fibroblasts and SSc fibroblasts. We next investigated the effect of IL-20 on type I collagen expression in TGFβ-treated normal fibroblasts. Exogenous IL-20 decreased basal collagen expression, and TGFβ could not induce collagen expression in the presence of IL-20 (Figure 4A), suggesting that IL-20 both suppresses the effect of TGFβ and reduces basal collagen expression. As expected, the protein expression of Fli-1 was increased by IL-20 in the presence of TGFβ (Figure 4B), while the mRNA expression levels of Smad3 and endoglin were decreased significantly (Figure 4C). We assume that IL-20 reduces basal collagen transcription via Fli-1 induction, while the down-regulation of Smad3 and endoglin may cancel the effect of TGFβ. The inhibition of collagen by IL-20 (Figure 4D), the induction of Fli-1 by IL-20 (Figure 4E), and the reduction of Smad3 and endoglin by IL-20 (Figure 4F) were also observed in SSc fibroblasts.

Effect of IL-20 on bleomycin-induced skin fibrosis in mice. Skin fibrosis induced by bleomycin injection in mice is used as a murine model of SSc (33). The epidermis of control mouse skin expressed IL-20, while IL-20 expression was decreased in bleomycin-treated mouse epidermis (Figure 5A), as seen in SSc skin. The expression of IL-20 in inflammatory cells or endothelial cells was slight and similar between control and

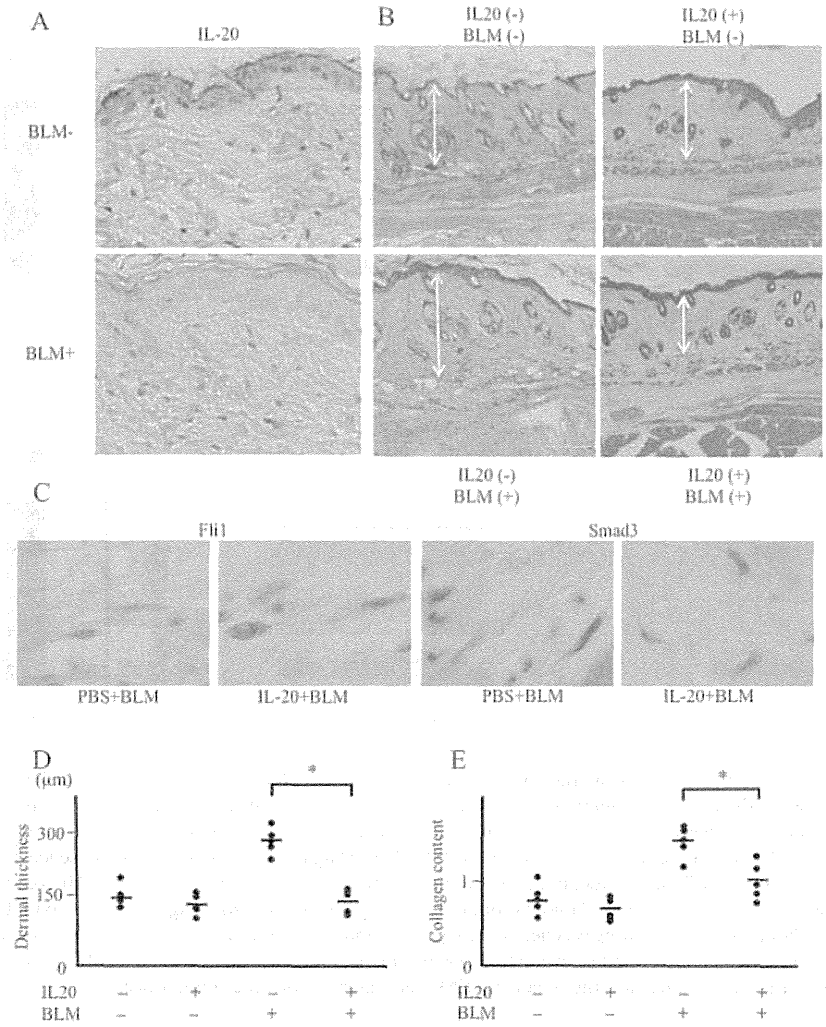

Figure 5. Effect of interleukin-20 (IL-20) on bleomycin (BLM)–induced skin fibrosis in vivo. **A,** Paraffin-embedded sections of skin were subjected to immunohistochemical analysis for IL-20. Top, Phosphate buffered saline (PBS)–treated wild-type mouse. Bottom, Bleomycin-treated mouse. Results shown are representative of 5 samples. Original magnification × 200. **B,** PBS- or bleomycin-treated mouse skin was injected with control PBS (left) or IL-20 (right) and stained with hematoxylin and eosin. **Double-headed arrows** indicate thickness of the dermis. Results shown are representative of 5 samples. Bars = 0.1 mm. **C,** Paraffin-embedded sections of bleomycin-treated mouse skin injected with control PBS or IL-20 were subjected to immunohistochemical analysis for Fli-1 or Smad3. Results shown are representative of 5 samples. Original magnification × 400. **D,** Dermal thickness was measured in PBS- or bleomycin-treated mouse skin injected with control PBS or IL-20 (n = 5 samples per group). Symbols represent individual samples; bars show the mean. * = $P < 0.05$. **E,** The amount of collagen content in skin sections was quantified using an assay kit (n = 5 samples per group). Symbols represent individual samples; bars show the mean. * = $P < 0.05$.

bleomycin-treated mouse skin. Accordingly, we tried to determine whether IL-20 supplementation could reverse skin fibrosis in SSc.

Bleomycin (300 μg) or control PBS was locally injected into the back of BALB/c mice 6 times per week for 1 month, and at the same time PBS or IL-20 (3.5 μg) was injected once per week (4 times per month) (further information available from the corresponding author). In the absence of bleomycin injection, IL-20 reduced dermal thickness slightly, but the difference was not significant. Bleomycin treatment without IL-20 induced dermal fibrosis with an increased number of thickened collagen bundles (Figure 5B). However, IL-20 reduced the extent of bleomycin-induced skin thickening (Figure 5B). In immunohistochemical staining using paraffin-embedded mouse skin sections, the expression of Fli-1 in fibroblast-like spindle cells was increased by IL-20, while the expression of Smad3 was decreased (Figure 5C),

consistent with in vitro results. We found that reversal of bleomycin-induced dermal thickening by IL-20 was statistically significant (Figure 5D). In addition, the increased amount of collagen induced by bleomycin in skin tissue was also significantly decreased by IL-20 (Figure 5E). Taken together, these results indicate that IL-20 supplementation could attenuate bleomycin-induced skin fibrosis.

DISCUSSION

In the skin, IL-20 is known to induce keratinocyte proliferation, but the effect on dermal fibroblasts has not been investigated. Our study revealed that $\alpha 2$(I) collagen mRNA expression was reduced by IL-20 at the transcriptional level, and that the decrease was mediated by Fli-1 induction in normal dermal fibroblasts. We did not determine the regulatory mechanism of the type I collagen $\alpha 1$ chain in the present study, but there may be similar mechanisms in IL-20–mediated $\alpha 1$(I) collagen down-regulation, because Fli-1 also controls $\alpha 1$(I) collagen expression (33).

There was a significant difference in serum IL-20 levels between patients with scleroderma spectrum disorders and normal subjects. As described above, scleroderma spectrum disorder is a prodromal stage of SSc, and a similar condition was also reported as "limited SSc" by LeRoy and Medsger (42). Because fibrotic change in SSc is usually irreversible, new strategies are needed to diagnose patients as early as possible and to follow them up carefully. For that purpose, the concept of scleroderma spectrum disorder is helpful. Serum IL-20 levels may be useful for differentiating patients with scleroderma spectrum disorders from normal subjects.

Generally, patients with scleroderma spectrum disorders lack a fibrotic response but show prominent clinical symptoms associated with vasculopathy (further information available from the corresponding author). Given that there have been a couple of articles regarding the role of IL-20 in angiogenesis (43,44), decreased serum IL-20 levels in patients with scleroderma spectrum disorders suggests that IL-20 is potentially linked to the pathogenesis of vasculopathy leading to the development of fibrosis. However, as the limitation of this study, scleroderma spectrum disorders potentially include undifferentiated connective tissue diseases developing into collagen diseases other than SSc. Therefore, it is basically impossible to say that all patients with scleroderma spectrum disorders included in this study have an established clinical entity that will develop into SSc. Longitudinal studies of serum IL-20 levels in patients with SSc developed from scleroderma spectrum disorders are needed in the future.

We found that IL-20 expression was decreased in SSc epidermis. We have a hypothetical model of IL-20–mediated tissue fibrosis in SSc (further information available from the corresponding author). Reduction of IL-20 expression in SSc skin may further down-regulation of Fli-1, with subsequent collagen overexpression in SSc fibroblasts; Fli-1 was reported to be constitutively decreased in SSc fibroblasts, probably due to TGFβ signaling (45), and reduction of IL-20 expression may enhance Fli-1 down-regulation. The addition of ectopic IL-20 reduces collagen expression effectively, via Fli-1 recovery and suppression of Smad3 and endoglin. In addition, the epidermis of SSc skin is known to become atrophic, and this may be because of reduced keratinocyte proliferation resulting from decreased IL-20. On the other hand, in psoriasis, IL-20 is thought to be overexpressed in epidermis and to lead to characteristic keratinocyte proliferation and epidermal thickening (13). This may explain why psoriasis skin is protected from dermal fibrosis despite chronic inflammation.

Our model indicates that IL-20 may have therapeutic value for the fibrotic condition of SSc. We were able to inhibit bleomycin-induced fibrosis by using IL-20 supplementation in the mouse model. To date, steroids, cyclophosphamide, and methotrexate are considered the first-choice drugs for treating the severe skin fibrosis of SSc (46,47). However, these conventional treatments usually have limited effects. Furthermore, these treatments are often accompanied by various significant adverse effects (48). Clarifying the mechanism by which IL-20 regulates tissue fibrosis in SSc skin may lead to a better understanding of this disease and to new therapeutic approaches. However, our study has other limitations involving potential contradiction of our in vivo results with our in vitro results. For example, further studies are needed to examine the function and expression pattern of IL-20R in murine dermal fibroblasts. Similarly, the data showing that the inhibitory effect of IL-20 on collagen was blocked by Fli-1 siRNA in vitro should be confirmed in vivo (i.e., the effect of IL-20 on bleomycin-induced dermal fibrosis in Fli-1–knockout mice should be determined).

AUTHOR CONTRIBUTIONS

All authors were involved in drafting the article or revising it critically for important intellectual content, and all authors approved the final version to be published. Dr. Jinnin had full access to all of the data in the study and takes responsibility for the integrity of the data and the accuracy of the data analysis.

Study conception and design. Jinnin, Asano, Trojanowska, Fukushima, Ihn.